OULU 2017
C 615

ACTA UNIVERSITATIS OULUENSIS

Mei-Yu Chen

ULTRA-LOW SINTERING TEMPERATURE GLASS CERAMIC COMPOSITIONS BASED ON BISMUTH-ZINC BOROSILICATE GLASS

UNIVERSITY OF OULU GRADUATE SCHOOL;
UNIVERSITY OF OULU,
FACULTY OF INFORMATION TECHNOLOGY AND ELECTRICAL ENGINEERING

ACTA UNIVERSITATIS OULUENSIS
C Technica 615

MEI-YU CHEN

ULTRA-LOW SINTERING TEMPERATURE GLASS CERAMIC COMPOSITIONS BASED ON BISMUTH-ZINC BOROSILICATE GLASS

Academic dissertation to be presented with the assent of the Doctoral Training Committee of Technology and Natural Sciences of the University of Oulu for public defence in the OP auditorium (L10), Linnanmaa, on 16 June 2017, at 12 noon

UNIVERSITY OF OULU, OULU 2017

Acta Univ. Oul. C 615, 2017

Supervised by
Professor Heli Jantunen
Docent Jari Juuti

Reviewed by
Professor Hsing-I Hsiang
Doctor R. Ratheesh

Opponent
Professor Hong Wang

ISBN 978-952-62-1559-4 (Paperback)
ISBN 978-952-62-1560-0 (PDF)

ISSN 0355-3213 (Printed)
ISSN 1796-2226 (Online)

Cover Design
Raimo Ahonen

JUVENES PRINT
TAMPERE 2017

Chen, Mei-Yu, Ultra-low sintering temperature glass ceramic compositions based on bismuth-zinc borosilicate glass.

University of Oulu Graduate School; University of Oulu, Faculty of Information Technology and Electrical Engineering

Acta Univ. Oul. C 615, 2017

University of Oulu, P.O. Box 8000, FI-90014 University of Oulu, Finland

Abstract

In the first part of the thesis, novel glass-ceramic compositions based on Al_2O_3 and $BaTiO_3$ and bismuth-zinc borosilicate (BBSZ) glass, sintered at ultra-low temperatures, were researched. With adequate glass concentration, dense microstructures and useful dielectric properties were achieved. The composite of $BaTiO_3$ with 70 wt % BBSZ sintered at 450 °C exhibited the highest relative permittivity, ε_r, of 132 and 207 at 100 kHz and 100 MHz, respectively. Thus, the dielectric properties of the composites were dominated by the characteristics of glass, $BaTiO_3$, and $Bi_{24}Si_2O_{40}$ phase, especially the contribution of $Bi_{24}Si_2O_{40}$ for the samples with 70-90 wt % glass. Actually, the existence of the secondary phase $Bi_{24}Si_2O_{40}$ may not hinder but enhance the dielectric properties. The Al_2O_3-BBSZ composition samples showed a similar situation, not only for densification but also for their microstructures and phases (Al_2O_3, BBSZ, $Bi_{24}Si_2O_{40}$) explaining the achieved dielectric properties.

The second part of the thesis mainly discusses the composite of $BaTiO_3$ with 50 wt % BBSZ with different thermal treatments. After sintering at 720 °C, dense microstructures and the existence of $Bi_4BaTi_4O_{15}$, $BaTiO_3$, $Bi_{24}Si_2O_{40}$ phases were observed. The results also showed that the size of glass powder particles did not influence the dielectric properties (ε_r = 263-267, tan δ = 0.013 at 100 kHz) of sintered samples, but the addition of LiF degraded the dielectric properties due to the features and amount of $Bi_4BaTi_4O_{15}$. These results demonstrate the feasibility of the BBSZ based composites for higher sintering temperature technologies as well.

At the end, a novel binder system, which enables low sintering temperatures close to 300 °C, was developed. A dielectric multilayer module containing $BaTiO_3$-BBSZ and Al_2O_3-BBSZ composites with silver electrodes was co-fired at 450 °C without observable cracks and diffusions. These results indicate that these glass-ceramic composites provide a new horizon to fabricate environmentally friendly ULTCC materials, as well as multilayers for multimaterial 3D electronics packages and high frequency devices.

Keywords: BBSZ glass, glass-ceramics, multilayers, sintering behaviour, Ultra-low Temperature Co-fired Ceramics (ULTCC)

Chen, Mei-Yu, Vismutti-sinkki borosilikaattilasiin perustuvat ultramatalassa lämpötilassa sintrattavat lasi-keraami komposiitit.

Oulun yliopiston tutkijakoulu; Oulun yliopisto, Tieto- ja sähkötekniikan tiedekunta

Acta Univ. Oul. C 615, 2017
Oulun yliopisto, PL 8000, 90014 Oulun yliopisto

Tiivistelmä

Väitöstyön ensimmäisessä osassa tutkittiin ja kehitettiin uudentyyppisiä, ultramatalissa sintrauslämpötiloissa (ULTCC) valmistettuja lasi-keraami komposiitteja käyttäen vismuttisinkkiborosilikaatti -pohjaista lasia (BBSZ). Täyteaineina olivat alumiinioksidi (Al_2O_3) ja bariumtitanaatti ($BaTiO_3$). Materiaaleille saatiin riittävän suuren lasipitoisuuden avulla tiheät mikrorakenteet ja sovelluskelpoiset dielektriset ominaisuudet. $BaTiO_3$:n komposiitti, joka sisälsi 70 p-% BBSZ lasia, saavutti 450 °C lämpötilassa sintrattuna korkeimman suhteellisen permittiivisyyden: ε_r=132 (@100 kHz) ja ε_r=207 (@100 MHz). Komposiittien dielektrisiä ominaisuuksia määrittivät tällöin lasi-, $BaTiO_3$- ja $Bi_{24}Si_2O_{40}$- faasien ominaisuudet ja erityisesti $Bi_{24}Si_2O_{40}$ -faasi näytteissä, joissa on 70-90 p-% lasia. Sekundäärinen faasi $Bi_{24}S_{i2}O_{40}$ ei välttämättä heikentänyt, vaan jopa paransi dielektrisiä ominaisuuksia. Vastaavilla Al_2O_3-BBSZ –komposiiteilla saavutettiin samanlaisia tuloksia tihentymisen, mikrorakenteiden ja faasien (Al_2O_3, BBSZ, $Bi_{24}Si_2O_{40}$) suhteen. Lisäksi tässä tapauksessa saavutetut dielektriset ominaisuudet voidaan selittää näiden kolmen faasin yhdistelmän olemassaololla.

Väitöstyön toinen osa käsitteli pääasiassa eritavoin lämpökäsiteltyjä $BaTiO_3$:n komposiitteja, joissa on 50 p-% BBSZ-lasia. Näillä saavutettiin tiheä mikrorakenne sintrattaessa 720 °C lämpötilassa ja havaitiin $Bi_4BaTi_4O_{15}$-, $Bi_{24}Si_2O_{40}$-faasien muodostuminen $BaTiO_3$ lähtöfaasin rinnalle. Tulokset osoittivat myös, että lasijauheen partikkelikoko ei vaikuttanut sintrattujen näytteiden dielektrisiin ominaisuuksiin (ε_r = 263-267, tan δ = 0.013 (@100 kHz)). LiF -lisäys sen sijaan heikensi dielektrisiä ominaisuuksia ja vähensi $Bi_4BaTi_4O_{15}$ faasin muodostumista. Tämä aiheutui $Bi_4BaTi_4O_{15}$-faasin ominaisuuksista ja oli riippuvainen kyseisen faasin määrästä. Nämä tulokset osoittivat BBSZ -pohjaisten komposiittien käytettävyyden myös korkeampien sintrauslämpötilojen teknologioihin.

Viimeisenä kehitettiin uudentyyppinen sideainesysteemi, joka mahdollistaa ultramatalien keraamien yhteissintraamisen jopa noin 300 °C lämpötilassa. Hyödyntäen kehitettyä sideainesysteemiä monikerrosrakenne, jossa käytettiin dielektrisiä $BaTiO_3$-BBSZ- ja Al_2O_3-BBSZ-komposiitteja ja hopeaelektrodeja, yhteissintrattiin 450 °C lämpötilassa. Valmistetuissa rakenteissa ei havaittu murtumia eikä diffuusioita. Tulokset osoittavat, että kehitetyt lasi-keraami komposiitit mahdollistavat ympäristöystävällisten ULTCC -materiaalien valmistuksen. Lisäksi osoitettiin kehitettyjen materiaalien soveltuvuus monikerroksisten rakenteiden käyttöön monimateriaali-3D-elektroniikan pakkauksissa ja suurtaajuuskomponteissa.

Asiasanat: BBSZ-lasi, lasikeraamit, monikerrosrakenteet, sintrautumiskäyttäytyminen, ultramatalan lämpötilan yhteissintrattavat keraamit (ULTCC)

Try not to be a man of success, but rather try to become a man of value. *Albert Einstein*

Acknowledgements

First of all, I would like to show my greatest gratitude to my supervisor Professor Heli Jantunen. You not only gave me the opportunity and resources to present this work, but also constructed the dual degree program between National Taiwan Normal University (NTNU) and University of Oulu. This program brought me here to Oulu, Finland, and enabled me to learn more from different points of view. Particularly, your support, encouragement, belief and positive thinking have been leading me along the way. I also want to thank my co-advisor Jari Juuti who offered me many constructive comments and reviewed my writings and reports. Prof. Chih-Ta Chia and Prof. Chi-Shuing Hsi are my important supports in Taiwan. They always gave the best academic suggestions, which helped me to solve practical questions.

This work was undertaken at the Microelectronics Research Unit and was a part of project funded by the European Research Council. Special thanks go to the Center of Microscopy and Nanotechnology and its staff for their technological support. Also, thanks to all group members, Timo Vahera, Tuomo Siponkoski, Hanna Kähäri, Jani Peräntie, Maciej Sobocinski, and Jobin Varghese for your assistance in this work and guidance of experiments and measurements together with your warm concern when I was falling into depression in the wintertime.

Thanks to Dr. Geza Toth and his wife Chia-Shan Yang, and the Chinese bible study group. They have been my personal support in Finland. I love you.

Finally, the most beloved thanks go to my family; my father and sister, without whose patience and understanding, this work could not have been done and the contribution of my mom in heaven. You gave me life, truth and love. Thanks.

Oulu, June 2017 Mei-Yu Chen

Symbols and abbreviations

LTCC	Low Temperature Co-fired Ceramics
ULTCC	Ultra-Low Temperature Co-fired Ceramics
CBS	$CaO-B_2O_3-SiO_2$ glass
BBSZ	$Bi_2O_3-B_2O_3-SiO_2-ZnO$ glass
XRD	X-ray diffraction
Ø	Diameter
T_g	Transition temperature of glass
T_s	Softening temperature of glass
T_c	Crystallization temperature of glass
A50-A90	(50-10) wt% $BaTiO_3$-(50-90) wt% BBSZ
A50n	50 wt% $BaTiO_3$ - 50 wt% BBSZ glass powder (particle size of 0.5 µm)
A50_LiF	50 wt% $BaTiO_3$ - 50 wt% BBSZ glass with 2 wt% LiF addition
a80-a90	$BaTiO_3$- BBSZ composites with 20-10 wt% and 80-90 wt%, respectively, sintered at 400 ^oC
B50-B90	(50-10) vol% Al_2O_3-(50-90) vol% BBSZ which was sintered at 450 ^oC
tan δ	Loss tangent
Qxf	Quality factor
ε_r	Relative permittivity
τ_f	Temperature coefficient of resonant frequency
PVB	PolyVinyl Butyral
QPAC®40	Polypropylene carbonate (EMPOWER)
DSC	Differential Scanning Calorimetry
TGA	ThermoGravimetric Analyzer
FESEM	Field Emission Scanning Electron Microscope
EDS	Energy Dispersive X-ray Spectrum

Original publications

This thesis is based on the following publications, which are referred to throughout the text by their Roman numerals:

I Chen Mei-Yu, Juuti Jari, Hsi Chi-Shiung, Chia Chih-Ta & Jantunen Heli (2015) Dielectric $BaTiO_3$-BBSZ glass ceramic composition with ultra-low sintering temperature. J Euro Ceram Soc 35(1): 139–144.

II Chen Mei-Yu, Juuti Jari, Hsi Chi-Shiung, Chia Chih-Ta & Jantunen Heli (2015) Dielectric properties of ultra-low sintering temperature Al_2O_3-BBSZ glass composite. J Am Ceram Soc 98(4): 1133–1136.

III Chen Mei-Yu, Juuti Jari, Hsi Chi-Shiung & Jantunen Heli (2017) Sintering behavior and characteristics study of $BaTiO_3$ with 50 wt% of B_2O_3-Bi_2O_3-SiO_2-ZnO glass. J Euro Ceram Soc 37(4): 1495–1500.

IV Chen Mei-Yu, Vahera Timo, Hsi Chi-Shiung, Sobocinski Maciej, Teirikangas Merja, Peräntie Jani, Juuti Jari, Jantunen Heli (2017) Tape Casting System for ULTCCs to Fabricate Multilayer and Multimaterial 3D Electronic Packages with Embedded Electrodes. J Am Ceram Soc 100(4): 1257-1260.

In Papers I & II, two glass ceramic composites based on BBSZ glass, sintered at ultra-low temperature (400 ^oC, 450 ^oC) are introduced, and their microstructures, crystal phases and dielectric properties at 100 kHz and 100 MHz are studied. Paper I mainly discusses the densities, phases, microstructures and dielectric performance of the $BaTiO_3$-BBSZ composite. The properties of the Al_2O_3-BBSZ composite are investigated in Paper II. Paper III reveals the effect of different heat treatments on $BaTiO_3$-BBSZ composite and the interactions between the glass and the dielectric powder at high temperatures. Additionally, Paper IV demonstrates a new binder system for tape casting which is suitable even for sintering temperatures of 300 ^oC. A multilayered structure consisting of alternating variable relative permittivity layers with silver electrodes is described.

The glass fabrication was done by the co-author, Chi-Shiung Hsi. The main ideas in Paper I and II were developed in association with the co-authors. The author has performed all the experiments and fabricated the composites and samples in Papers I-III. The multimaterial module in Paper IV was prepared by the author with the kind assistance of co-authors. The slurry composition for tape casting was developed by one of the co-authors (Timo Vahera). The manuscripts of Paper I-IV were written by the author with the kind help of the co-authors.

Contents

1 Introduction

1.1 Ultra-Low Temperature Co-fired Ceramics (ULTCC)

Low Temperature Co-fired Ceramics (LTCC) play a key role in the modern communications industry. The multilayer co-fired technology is used to fabricate several devices such as band pass filters, oscillators, waveguides and antennas for the miniaturization of microwave components with enhanced reliability. The modules, containing the green LTCC dielectric tape, passive components and silver electrodes, are co-fired below the melting point of the silver electrodes (961 ^{o}C). Actually most of the LTCC materials are sintered at temperatures in the range 700 ^{o}C-1000 ^{o}C and are important for the rapidly developing industry market. Currently, novel materials with much lower sintering temperatures are attracting attention in science and in industrial sectors [1–2]. These materials with ultra-low sintering temperature (<700 ^{o}C) help to reduce energy consumption and enable feasible usages and integrations with other materials such as low melting-point electrodes, semiconductors such as silicon or GaAs, and polymer based substrates [3].

The first reported Ultra-Low Temperature Co-fired Ceramics (ULTCC) material was from the Valant and Suvorov group in 2001 [4]. They reported that $Bi_{12}PbO_{19}$ sillenite could be sintered at 680 ^{o}C and it exhibited a relative permittivity (ε_r) of 38.6, a low Qxf value of 2900 GHz and temperature dependence of resonance frequency (τ_f) of -84 ppm/^{o}C at 5.5 GHz. Since then it has been found that there are several other potential low melting candidate systems for ULTCC, such as various glass-ceramic/glass+ceramics, bismuth Bi_2O_3-, tellurate TeO_2-, vanadate V_2O_5-, tungstate WO_3-, molybdate MoO_3-, and borate B_2O_3-based composites [3-10].

Recently Zhou *et al.* reported many new ULTCC microwave ceramics based on Li_2O-Bi_2O_3-MoO_3 and ABO_4-related (A=Li, Na, K, Bi, Zn, Rb; B=Mo, V) systems, whose sintering temperatures are around 530-700 ^{o}C [5-6]. Kwon *et al.* reported that Te-rich compositions in the BaO-TeO_2 binary compounds system have good dielectric properties (ε_r = 17.5, Qxf = 54 700 GHz at 12 GHz) with a sintering temperature of 550 ^{o}C [7]. Additionally Wang *et al.* [8] reported that $Te_2(Mo_{1-x}W_x)O_7$ can be sintered at 520 ^{o}C and has acceptable dielectric properties (ε_r = 13.6, Qxf = 46 900 GHz for x=0, ε_r=13.9, Qxf =25 820 for x=0.05). However, compatibility with the silver electrodes is a severe issue for practical applications. Many of these compounds react with commercial silver pastes. Other problems are

toxicity and hazardousness for the environment. Pb-, Te- and V- related element composites are proven to be harmful for humans and environments [9]. Recently, some research has been reported which aims for environmental friendly ULTCC ceramics. In the case of MoO_3-based composites, Liu *et al*. reported that a 15 - 20 μm $Bi_2Mo_2O_9$ thick film printed on Al foil can be sintered at 645 °C and achieve ε_r ~ 38 and tan δ of ~ 0.007 at 100 kHz [10].

1.2 Glass ceramics in LTCC and ULTCC

Glass-ceramic composite (glass+ceramic) and glass-ceramics (crystallizable glass) are essential for modern technology although they were found accidentally in 1953. There are many applications for them due to their unique characteristics of dielectric properties suitable for electronics, high mechanical strength and chemical durability for dental appliances, low thermal expansion coefficient and high resistance to thermal expansion for various types of cooking ware, and so on [11]. For LTCC applications, numerous technologies were developed such as multilayer microwave components and hermetic sealing of packages, sensors, or other devices. Sebastian and Jantunen have provided an excellent review and extensively discussed the commonly used glass types in the LTCC regime [2]. The glass–ceramics were derived from a glassy system and partly crystallized during the sintering process. The degree of crystallization, which is controlled by the addition of suitable nucleating agents, dominates the properties of glass–ceramic. The sintering temperatures of glass–ceramics are commonly in the range 700 – 1000 °C with the softening temperature of initial glasses in the range 650 – 710 °C. Crystallizing cordierite (IBM) and wollastonite (Ferro Corporation) are examples of such glass-ceramic systems. Glass+ceramic is made from a low melting glass with a crystallized dielectric ceramic filler. The liquid glass wets the crystalline powder above the softening temperature of glass and enhances the densification. The sintered ceramics are usually multiphase and their properties depend on the characteristics of individual phases and on the level of densification, crystallinity, and their microstructure. $CaO–B_2O_3–SiO_2$ (CBS) glass is an extensively used glass for LTCC applications [3, 12-15]. Wang *et al.* prepared CBS glass with different molar ratios and reported the dielectric properties of CBS glass-ceramics sintered around 850-1000 °C. After firing, the commercial product, which exhibits a crystallization phase of $CaSiO_3$ and residual borosilicate glass, is used in military and aerospace applications at 20-30 GHz due to its low dielectric loss. Also CBS glass is applied in glass-ceramic composites as an additive. Hsi *et al.* reported that

CBS glass coated $BaTiO_3$ efficiently enabled a decrease in the sintering temperature from 1450 °C to 850 °C [14-15].

Recently, the rapidly growing electronic industry has increasingly encouraged the search for low melting glass (T_s < 700 °C) for more practical applications. The microwave dielectric properties of MO–B_2O_3–SiO_2 (M = Mg, Ba or Sr) glasses which have a softening temperature (T_s) in the range 560–613 °C have been reported [16]. Additionally, the characteristics of ZBS (ZnO–B_2O_3–SiO_2), BBS (BaO–B_2O_3–SiO_2), PBS (PbO–B_2O_3–SiO_2) glass were investigated by Wu and Huang [17]. The ZBS and BBS glasses have a T_g in the range 550–720 °C depending on the compositions, while PBS glass has a lower T_g in the range of 312–500 °C. Rajesh *et al*. [18] proposed two similar glass ceramics, (50 wt% glass + 50 wt% Al_2O_3) and co-fired with silver electrodes. These two commercial glasses, G018-249 and G018-250, were selected and have the glass transition temperatures T_g of 365 and 380 °C respectively. G018-249 glass contains a large amount of Bi_2O_3 and ZnO while high contents of Li_2O and Bi_2O_3 are included in the G018-250 glass. The composites were sintered at 650 °C and no reaction with silver electrode was observed. In addition, they showed a relative permittivity of 9.5 and 8.85 and loss tangents 0.0068 and 0.0087 at 1 MHz respectively. 3ZnO–$2B_2O_3$ glass ceramic sintered at 650 °C for 0.5 hr was reported by Yu and co-workers [19]. The glass with an addition of 15 wt% SiO_2 has ε_r of 6.1 and tan δ of 0.0013 at 1 MHz. Moreover, laminated 5-layer tapes of this composite were sintered at 650 °C obtaining dielectric properties (ε_r = 6.4, tan δ = 0.001) quite close to those of the bulk samples. Furthermore, Honkamo *et al.* proposed the first ULTCC tapes of TiO_2 doped $Zn_2Te_3O_8$ composites in 2009. The slurry was prepared with a well-known LTCC binder system and the laminated tapes were sintered at 660 °C [20].

1.3 Literature survey of BBSZ glass and related ceramics composites with BBSZ glass

In order to meet the requirements for LTCC fabrication, an abundance of glass systems have been developed. Lead-containing glasses are one of most popular systems and have been applied for decades. However, since PbO was proven to be toxic to humans and animals and PbO-containing electronic waste is damaging to the environment according to the Regulation of Restriction of Hazardous Substances directive (RoHS), scientists searched for alternative elements to replace lead in electronic materials. Bi_2O_3 is one of the potential candidates due to its similar highly polarizability and isoelectronic characteristics [21]. The first attempt

to fabricate the Bi_2O_3-B_2O_3-SiO_2-ZnO (BBSZ) quaternary system started in 1980. A series of early Soviet scientists [22-24] prepared a class of low-melting or intermediate glass frits with various additions. They claimed that this glass system exhibited good chemical resistance and a lower CTE than Pb-containing glass. Later many patents and applications were developed incorporating BBSZ related composites for applications in glazing & enamels, TF conductors, resistors and over glazes, plasma display panel dielectrics, conductors and low-melting point sealing [23]. These patents not only reported on transition temperatures (T_g), softening temperatures (T_s) and temperature coefficients (CTE), but also on the durability, hardness, and electrical conductivity. The content of Bi_2O_3 plays a key role in making amorphous glass. The US patents from Hasegawa *et al.* [25] extensively discussed the applicable fabricating region of BBSZ glass and the effects of similar compositions with various additives. Furthermore, a higher amount of Bi_2O_3 lowers the T_g point, but this decreases the stability of glass. Dyamant *et al.* [26] also studied the thermal properties of a BBSZ system (40-60 mol% of SiO_2, 10-45 mol% of Bi_2O_3, 10-30 mol% of B_2O_3, 1-35 mol% of ZnO). The composition of BBSZ glass in this thesis is 27 mol% B_2O_3, 35 mol% Bi_2O_3, 6 mol% SiO_2 and 32 mol% ZnO.

The first attempts to utilize this BBSZ glass in LTCC fabrication to lower the sintering temperature were made by Dernovsek *et al.* [27] in 2001. 10 vol% BBSZ glass addition to $BaNd_2Ti_4O_{12}$ microwave ceramics can be densified at 880 ^oC. Later, many composites with different amounts of BBSZ were sintered at around 850-950 ^oC, including dielectric, ferromagnetic, ferroelectric, and ferrite materials [28-31]. Thomas *et al.* showed that by the addition of 10 wt% of BBSZ glass to $0.83ZnAl_2O_4$-$0.17TiO_2$ the composite could be sintered at 900 ^oC, being stable with silver and exhibited $\varepsilon_r = 10$ and Qxf = 10,000 GHz [28]. Hsiang *et al.* reported that BNBT dielectrics-NiCuZn ferrite with 20 wt% of BBSZ glass sintered at 950 ^oC performed with excellent dielectric and magnetic properties in a broad frequency range. However, these studies regarded the glasses as additives and the sintering temperature of these compositions were higher than 800 ^oC. This is useful in LTCC but insufficient for ULTCC applications.

1.4 Scope and outline

The main goal of this thesis is to provide a series of ultra-low temperature sinterable glass ceramic composites with sintering temperatures below 700 ^oC and to study the interaction behaviour between glass and dielectric materials during liquid phase

sintering. The chosen BBSZ glass is proven to be effective at a lower sintering temperature. These compositions with different filler ceramic provide widely adjustable dielectric properties with different amounts of glass. Furthermore, a multimaterial multilayer module is demonstrated based on the composites in this thesis.

Chapter 1 of this thesis describes the state of the art of ultra-low sintering temperature ceramics. In addition, a literature study of BBSZ glass and related materials is included.

Chapter 2 presents the designed composites based on a BBSZ glass matrix. The essential experimental techniques and methodologies used in this thesis are also described. The main experimental results are shown and discussed in Chapter 3. In Section 3.1 and 3.2, the characteristics of $BaTiO_3$-BBSZ and Al_2O_3-BBSZ composites are studied with different amounts of BBSZ glass. The effects of the sintering temperature, glass particle size and fluoride addition on $BaTiO_3$-BBSZ composites are discussed in Section 3.3. Additionally, a multilayer module of $BaTiO_3$-BBSZ and Al_2O_3-BBSZ, described in Section 3.4, was successfully fabricated with a new binder system by the tape casting method.

Chapter 4 summarizes the main results of this work and shows the possible impacts on science and industry.

2 Developed composites and experimental methods

2.1 Chosen materials and developed composites

Al_2O_3-BBSZ composites

Corundum (α-Al_2O_3) is one of the most popular materials for industrial applications. It is widely used in spark plugs, which are required to have a combination of good thermomechanical and electrical properties, and klystrons and magnetrons for the generation of electromagnetic energy. Very pure Al_2O_3 (> 99.9%) exhibits ε_r and tan δ values between 9.8-10.1 and 0.00004-0.0002 at 1 MHz [32]. It is also extensively employed for thick film circuit substrates in microwave and millimetre wave communication and integrated circuit packaging. The typical sintering temperature of Al_2O_3 is around 1700 ^oC, which is too high to allow multimaterial integrations. [2, 33]. Therefore, doping with low melting point glass on Al_2O_3 ceramics is a good way to decrease the sintering temperature below 1000 ^oC and hence to integrate it with modules and silver electrodes. Several LTCCs based on Al_2O_3, and sintering aids such as La_2O_3-B_2O_3 glass, ZnO-B_2O_3-SiO_2 (ZBS) and B_2O_3-Bi_2O_3-SiO_2-ZnO (BBSZ) glass, have been developed [2]. In this thesis, compositions of *x* vol% Al_2O_3- (100-*x*) vol% BBSZ glass, where *x* = 10-50, were fabricated. The densities, crystal structures, microstructures and dielectric properties of such composites were explored in Paper II.

$BaTiO_3$-BBSZ composites

Since it was discovered in 1945 $BaTiO_3$ has becomes well-known not only for its high relative permittivity value, but also for its versatile piezoelectric and ferroelectric properties. It has been used in a diversity of applications, such as multilayer ceramic capacitors and transducers. The typical sintering temperature of bulk $BaTiO_3$ is higher than 1300 ^oC [34]. Therefore, numerous sintering aids and glass compositions have been used with $BaTiO_3$ and Ba-based materials in order to fabricate with LTCC modules [2]. For the BaO-TiO_2 system, the addition of 10 wt% of lithium based glass (10-35 wt% of SiO_2, 23-43 wt% of B_2O_3, 33-51 wt% of Li_2O) decreased the sintering temperature to 900 ^oC with a density of 98%, relative permittivity ε_r of 32, Qxf of 9 000 GHz and temperature dependence of resonance

frequency, τ_f , of 10 ppm/K [35]. In this thesis, the compositions, *x* wt% $BaTiO_3$-(100-*x*) wt% BBSZ glass for *x* = 10-50, were prepared. The sintering behaviour, densities, crystal structures, and microstructures, and dielectric characteristics were studied in Paper I and III.

2.2 Fabrication of composites

Reagent grade chemicals of B_2O_3 (Nippon Shiyaku Kogyo, Japan), Bi_2O_3 (Panreac, Spain), SiO_2 (Panreac, Spain), and ZnO (Nippon Shiyaku Kogyo, Japan) were used to prepare the BBSZ glass with a composition of 27 mol% B_2O_3, 35 mol% Bi_2O_3, 6 mol% SiO_2 and 32 mol% ZnO. The weighed and mixed raw materials were melted in a platinum crucible at 900 ^oC for 1 hr, quenched in water to form an amorphous glass, dried and crushed. The glass powder was obtained by planetary milling with deionized water and zirconia balls for 24 hrs. Two different batches with 0.5 μm and 1.1 μm particle size were prepared. Pure BBSZ disks were fabricated at 400 ^oC to keep them under the deformation temperature.

The composites based on the BBSZ glass matrix with the addition of Al_2O_3 (Alfa Aesar, MA, α-phase, 99.9%, mean particle size 1.1 μm) from 10 to 50 vol% and $BaTiO_3$ (Alfa Aesar, MA, 99.7%, mean particle size 0.94 μm) from 10 to 50 wt% were prepared separately; each of them was mixed with ethanol and a small amount (~ 0.25 wt%) of Menhaden oil (Grade Z-3, Richard E. Mistler, Inc.) as dispersant. All powders used had irregular shape. The slurry was mixed in an alumina container with alumina balls by planetary milling for 4 hrs without any binders. After drying, the mixed powder was pressed into pellets with a diameter of Ø 10 and 20 mm and thickness of 1-2 mm. The green densities of the specimens were 50-60% of their theoretical densities. The pressed composite disks were sintered with a heating rate of 3 ^oC/min and cooling with the furnace. The samples of BBSZ glass with (10-50) wt% $BaTiO_3$ and with (10-50) vol% Al_2O_3, which were sintered at 450 ^oC for 0.5 hr, were labelled as A50-A90 and B50-B90, respectively. Meanwhile, the samples of $BaTiO_3$ with 80 and 90 wt% of BBSZ glass sintered at 400 ^oC were denoted as a80 and a90, respectively. Additionally, another batch of the glass powder (n-BBSZ) was prepared by WAB Dyno-mill with 0.3 mm zirconia balls to achieve a smaller particle size (mean particle size 0.5 μm). The BBSZ glass and n-BBSZ glass powder was added to 50 wt% $BaTiO_3$ powder. These two batches were divided into three powder samples. The first sample was pressed into Ø=10 mm pellet and directly sintered, while the second one was pre-heated at 390 ^oC for 0.5 hr and then pressed into pellets and sintered. The third powder sample was

mixed with 2 wt% LiF, pressed into pellets and sintered. The same procedure was performed in both cases of the BBSZ glass. The samples were sintered at 450 °C for 0.5 hr and at 720 °C for 5 hrs with a heating rate of 3 °C/min using the conventional sintering process. The preparation routes of the samples are depicted in Fig. 1.

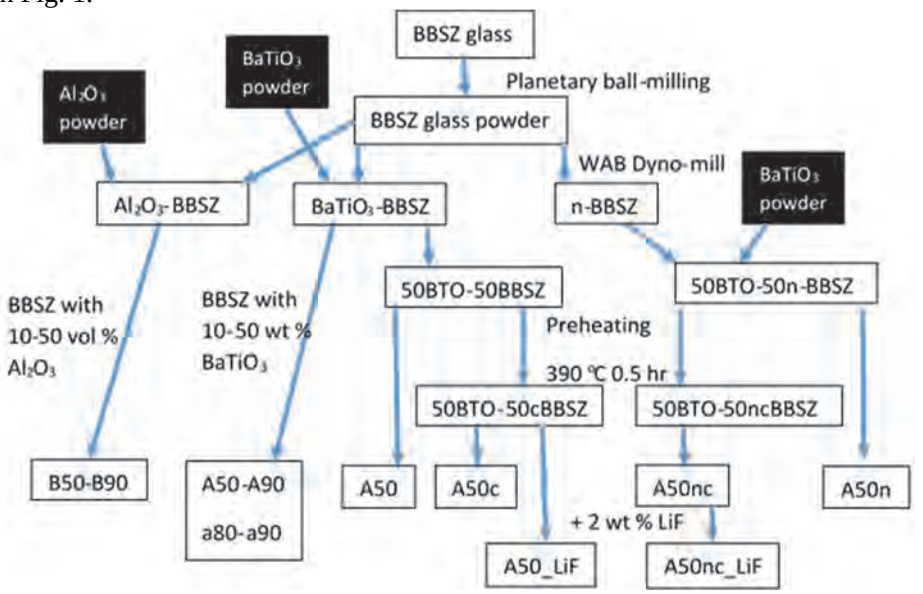

Fig. 1. The manufacturing route of samples.

Multimaterial tape fabrication

The route of the multimaterial layers fabrication processes of 30 wt% $BaTiO_3$- 70 wt% BBSZ and 30 vol% Al_2O_3-70 vol% BBSZ glass ceramics is shown in Fig. 2. The slurry was prepared by mixing the glass ceramic powder with solvent, plasticizers and a binder for 15 hrs. Dimethyl carbonate (DMC, Sigma-Aldrich, USA) was used as the solvent. The binder was polypropylene carbonate (QPAC40, EMPOWDER, USA), and the plasticizers were butyl benzyl phthalate (S160, Richard E. Mistler, Yardley, USA) and polyalkylene glycol (UCON 50HB2000, Richard E. Mistler, Yardley, USA). The binder selected was QPAC40 (molecular weight ~30 000) since it has low decomposing temperature (~ 180 °C). The slurry composition is presented in the weight and volume ratios of powders in Table 1.

The amount of the solvent was separately adjusted taking into account the binder system.

The tapes were cast on silicone coated Mylar™ using a laboratory caster (Unicaster 2000, Leeds, U.K.) with a single 400-µm-wide doctor blade and a casting speed of 0.8 m/min. The tapes were dried for 5 hrs using a metallic lid cover before releasing the tapes and further handling. The thickness of the cast green tapes was 110 µm. Silver electrodes (599-E, ESL Europe, UK) were screen printed on the surface of the green tapes and dried for 24 hrs at room temperature. Six to ten layers of tapes were stacked and hot isostatic laminated at 75 °C and 80 MPa for 10 min. The green density of the laminated stack was about 2.5 g/cm^3. Silver paste printed tapes were placed on the top and in the middle of the stack. Laminated multimaterial modules of 6 - 10 layers with $BaTiO_3$-BBSZ and Al_2O_3-BBSZ were then fabricated. The binders were burn out from laminated modules and sintered with a porous alumina plate on the top. The thicknesses of the fired electrodes were around 10-18 µm.

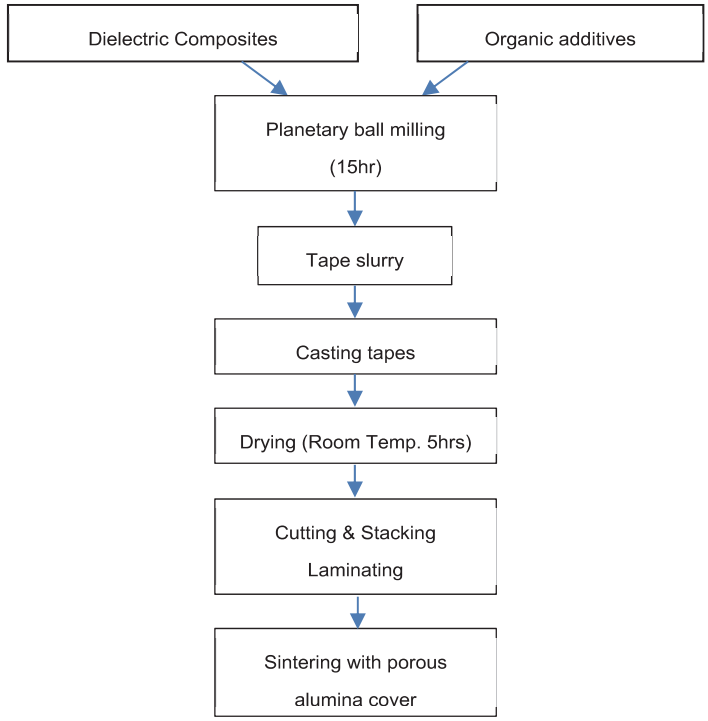

Fig. 2. The route of tape casting.

Table 1. Slurry compositions for tape casting of $BaTiO_3$-BBSZ and Al_2O_3-BBSZ composites (Paper IV, published by permission of John Wiley and Sons).

Glass ceramics		Dielectrics	QPAC40	S160	UCON	DMC
Al_2O_3-BBSZ	wt%	89.4	7.4	1.6	1.6	71.5
	vol%	66.5	22.5	5.4	5.6	255
$BaTiO_3$-BBSZ	wt%	89.5	7.0	1.7	1.7	69.8
	vol%	61.8	24.2	6.8	7.2	285

2.3 Density, phase identification, particle size, and microstructures

The bulk densities of the sintered samples were measured by the Archimedes method. A pycnometer was utilized to measure the true densities of the specimens. Before determining the true density, the sintered samples were broken and sieved into powder through a 90 μm mesh in order to remove the open and closed pores in the samples so that the true densities could be measured correctly. The average particle size of the glass powder was estimated using a particle size analyzer (Beckman Coulter LS 13 320, CA, USA).

The crystal structures of the samples were identified by X-ray diffractometers (Bruker D8, Cu, Kα ~ 1.5406 Å, MA, USA with Diffrac.Suite™ software and XRD, Rigaku, Co, Kα ~ 1.79 Å, Tokyo, Japan with PDXL software) and a Raman spectrometer (Horiba Jobin-Yvon LabRam HR800, 488 nm Ar^+ laser, France).
The Field Emission Scanning Electron Microscope (FESEM) analyses were undertaken with ZEISS Ultra Plus and Zeiss Sigma electron microscopes (Carl Zeiss, Germany). The elemental analysis and phase clarification was carried out by an energy dispersive x-ray spectrometer (EDS). Cross-sections were used in order to observe the microstructure of the samples or the multimaterial layers.

2.4 Dielectric and Thermal characterization

The parallel plate capacitance (C_p) and loss tangent of sandwiched capacitor samples were measured by a Precision LCR meter (LCR, HP 4284, USA) in order to obtain the relative permittivity values of samples at 100 kHz at a signal amplitude of 1 V_{rms}. Dielectric properties at 100 MHz and 1 GHz were measured by an impedance analyzer (Agilent, E4991A, USA) with E4991A-002 kit for material measurements. RF-sputtered silver electrodes were used to improve the reliability of the measurements. Round-shaped silver electrodes were deposited on the top (Ø =10 mm) and bottom (Ø =7 mm) surface of samples in an argon reduced

atmosphere (~ 10^{-3} torr) by a physical vapour deposition (PVD) System (Torr International Inc., NY, USA). The standard deviation values in all dielectric measurements were less than one percent. The accuracy of measured values of relative permittivity and tan δ depends on the frequency and the thickness of samples according to the measurement equipment manuals [36-37]. In particular, the accuracy of the dielectric measurements is not high with the impedance analyzer and especially at high frequencies.

The thermal analysis of selected composites was revealed by a dilatometer (Netzsch DIL402-PC, Germany) and a high-temperature differential scanning calorimeter (Netzsch 404 F3, Germany). The DSC/TGA measurements not only obtained the phase transformation behaviour of the BBSZ glass but also investigated the loss of mass of organic additives for tape casting. Rod-shaped (Ø = 5mm) green samples were prepared for dilatometry measurements.

3 Results and discussions

This chapter introduces and discusses the main results obtained in this thesis work. Detailed results can be found in the related publications of Paper I-IV.

3.1 The properties of BBSZ glass

The properties of BBSZ glass utilized in this thesis have to be studied before preparing the glass-ceramic composites. The true density of pure BBSZ glass was measured by pycnometer to be 6.85 g/cm^3. This high density is due to the heavy bismuth element. The thermal behaviour of the BBSZ glass powder and bulk samples was revealed from the scanning calorimetric and the differential curves (Fig. 3). Table 2 summarizes the transition temperatures (T_g), softening temperature (T_s), and crystallization temperature (T_c) of the BBSZ glass with different particle sizes and fluoride addition. The T_g of the BBSZ glass with mean particle sizes of 1 µm and 0.5 µm (denoted as n-BBSZ) were at around 382-386 ^{o}C. The T_s for these two sizes of glass powder was around 416 ^{o}C, while the addition of LiF decreased it to 408 ^{o}C. The exothermal peaks in Fig. 2(a) representing the T_c of the glass were 483 ^{o}C for the BBSZ bulk, 462 ^{o}C and 430 ^{o}C for the BBSZ and n-BBSZ powders, respectively. The results show that the smaller particle size markedly decreases the T_c of glass. Furthermore, the fluoride addition further assists to lower T_c of n-BBSZ to the value of 423 ^{o}C [Paper III].

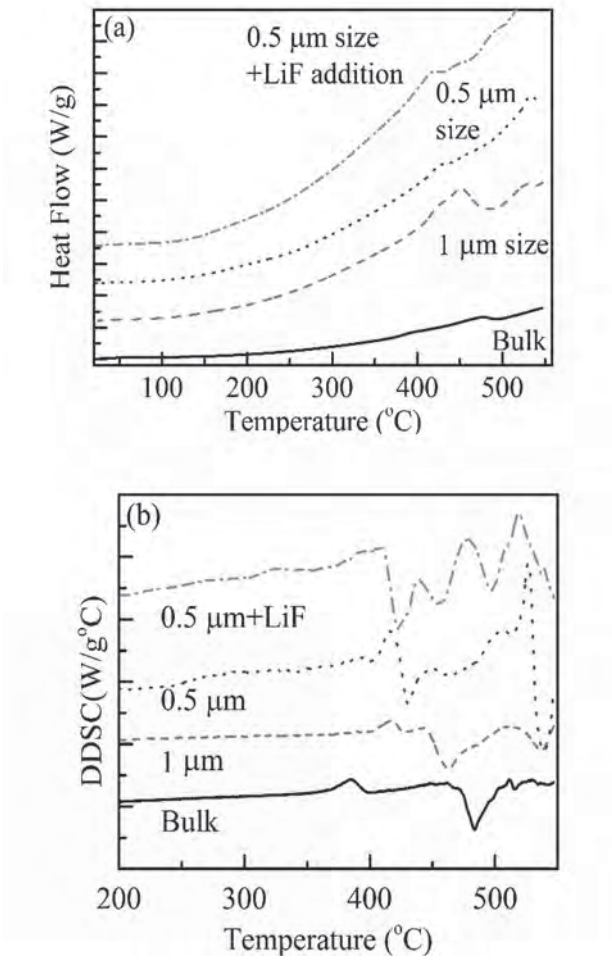

Fig. 3. (a) DSC and (b) differential curves of BBSZ glass with different particle sizes and LiF additions. (Paper III, published by permission of Elsevier).

Table 2. The transition, softening and crystallization temperature of BBSZ glass.

BBSZ Glass	Bulk	1 µm	0.5 µm	0.5 µm+LiF
Tg (°C)	384	382	386	386
Ts (°C)	NA	417	416	408
Tc (°C)	483	462	430	423

Fig. 4 shows the XRD patterns of BBSZ glass heated at 400, 450 and 720 °C. The hump at 20 - 35° clearly shows an amorphous glass phase with a heating temperature of 400 °C. $Bi_{24}Si_2O_{40}$ phase can be observed especially after sintering at 450 °C. In addition, Zn_2SiO_4 silicate phase was found in BBSZ glass heated at 720 °C [Paper III]. Existence of these phases depend also on the amount Bi in the system.

Moreover, the dielectric properties of pure BBSZ glass sintered at 400 °C for 0.5 hr were obtained ($\varepsilon_r \sim 28$, $\tan\delta \sim 0.005$ at 100 kHz, $\varepsilon_r \sim 42$, $\tan\delta \sim 0.02$ at 100 kHz, $\varepsilon_r \sim 46$, $\tan\delta \sim 0.023$ at 1 GHz). These results provide the basic information for further research into glass-ceramics composites based on BBSZ glass [Paper I-III].

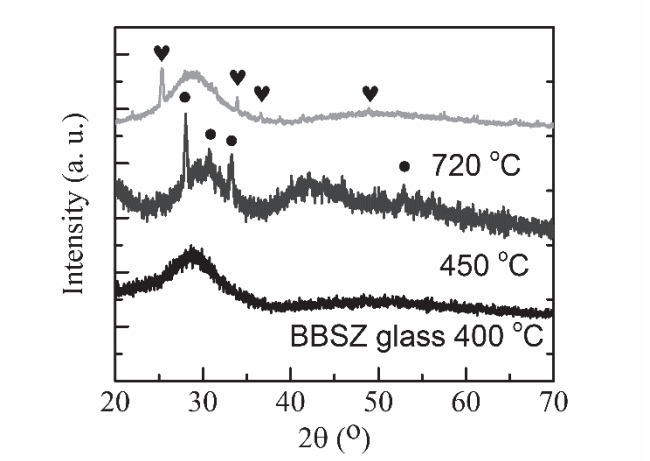

Fig. 4. XRD pattern of BBSZ glass heated at 400 °C, 450 °C and 720 °C (♥ refers to Zn_2SiO_4 and ● refers to $Bi_{24}Si_2O_{40}$) (Paper III, published by permission of Elsevier).

3.2 $BaTiO_3$-BBSZ composites

In order to study the compositions of (10-50) wt% $BaTiO_3$-(90-50) wt% BBSZ glass, a series of experiments was performed to investigate the shrinkage behaviour, the phases, microstructures, and dielectric properties of composites.

The dilatometry data of $BaTiO_3$ with 50-70 wt% of BBSZ glass (Fig. 5) show that the shrinkages of the samples began at about 382 - 386 °C, which is in same temperature range as the transition temperature (T_g) in Fig. 3. The shrinkage rates increased with the amount of the glass, and reached around 20% for the sample of $BaTiO_3$ with 70 wt% of glass addition. Fig. 5(b) reveals the slopes of the shrinkage

rate and shows that the sample with 70 wt% of glass had the sharpest peak. It suggests that a lower sintering temperature and shorter dwelling time is needed for this sample. The dilatometry data for the samples with 80 wt% and 90 wt% amount of glass are not shown because the results were very similar to those of the 70 wt% sample. The results clearly show that the densification of the samples was promoted even at low temperatures and a short dwell time [Paper I].

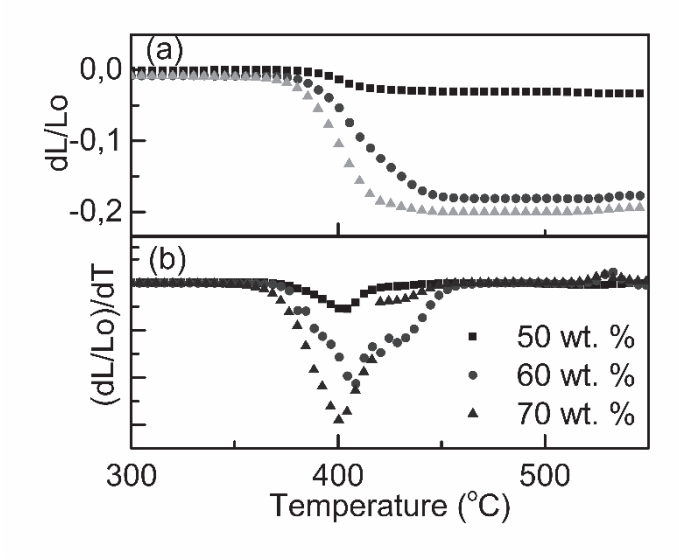

Fig. 5. (a) Dilatometric curves and (b) their derivation of $BaTiO_3$ with 50-70 wt% of BBSZ glass (Paper I, published by permission of Elsevier).

Fig. 6 illustrates the bulk densities of $BaTiO_3$ with 50-90 wt% BBSZ glass sintered at 450 ºC and 400 ºC. $BaTiO_3$ samples with 50-90 wt% of BBSZ glass sintered at 450 ºC are labelled as A50-A90 and the samples with 80 and 90 wt% of glass sintered at 400 ºC as a80 and a90. In Fig. 6, A70-A90 and a90 exhibit high bulk densities which reach values over 5.7 g/cm^3. The dashed line in Fig. 6 represents the ideal densities of samples which were calculated based on the densities of BBSZ glass (6.85 g/cm^3) and $BaTiO_3$ powder (5.85 g/cm^3), respectively. Moreover, the same compositions A90 and a90, a90 had a significantly lower bulk density. This could be expected due to the lower sintering temperature. Interestingly, the bulk densities of A80 and A90 were even larger than their calculated ideal density. This result implies the existence of an extra phase [Paper I].

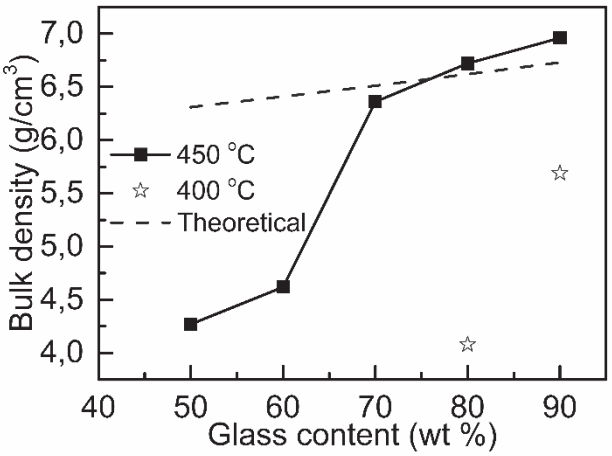

Fig. 6. The bulk densities of A50-A90 (squares) and a80-a90 (stars) (Paper I, published by permission of Elsevier).

XRD patterns of a90 and A50-A90 are shown in Fig. 7(a) and (b), respectively. Fig. 7a) shows the typical $BaTiO_3$ structure (peaks denoted with stars) and a large amount of amorphous background which is distributed at 20-35 °. No extra phases in the a90 and A50 sample could be found. However, an extra unknown peaks (marked as x) was observed in the samples of A60-A90 in Fig. 7(b). When the intensities of the $BaTiO_3$ peaks decline with higher glass content, the intensity of the glass background increase. In addition the peak indicating the new phase is the most prominent for the sample A90. Thorough analysis indicates that possible candidates for the new phase could be Bi_2O_3 or $Bi_{24}Si_2O_{40}$. The difficulty in distinguishing these phases was due to their similar lattice constant (a=10.1 Å), volume (V=1034 $Å^3$) and the same symmetry (I23). Therefore, more experiments are needed [Paper I].

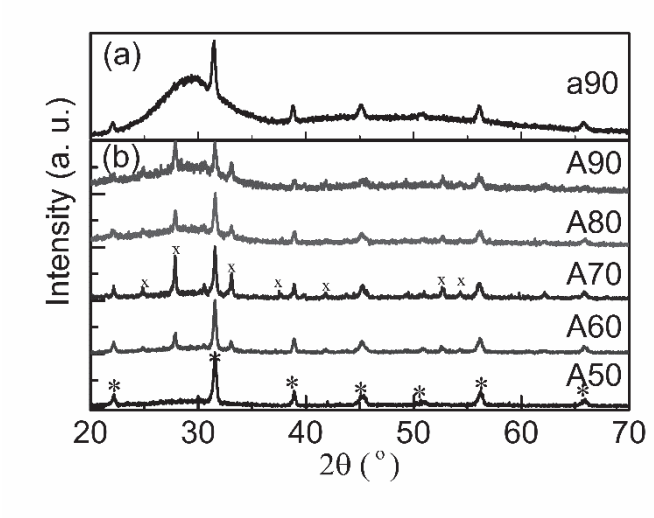

Fig. 7. XRD patterns of *x* wt% of BBSZ glass and (100-*x*) wt% of $BaTiO_3$ from *x*= 50-90 sintered at (a) 400 °C and (b) 450 °C. Stars denote the peaks of $BaTiO_3$ phase and peaks marked with x correspond to Bi_2O_3 phase (PDF 74-1375) or $Bi_{24}Si_2O_{40}$ (PDF 80-0627) (Paper I, published by permission of Elsevier).

Raman spectra of $BaTiO_3$ with 50-90 wt% glass composites are shown in Fig. 8. The typical tetragonal $BaTiO_3$ phase was observed in A50 and a80 and a90 samples. The results correspond to the XRD results with no extra phases after sintering. However, extra Raman peaks not belonging to $BaTiO_3$ (marked with arrows in Fig. 8) were detected in the A60-A90 samples being the highest for the sample A90. The Raman modes of the $BaTiO_3$ phase did not change with the increasing glass concentration. The best corresponding phases were γ-Bi_2O_3 or $Bi_{24}Si_2O_{40}$ [38]. In fact, $Bi_{24}Si_2O_{40}$, called sillente, forms a class of stabilized derivatives of γ-Bi_2O_3, which is iso-structural with γ-Bi_2O_3. This γ-Bi_2O_3 phase is ordinarily observed in samples that are annealed at 750 °C, but the impurity of Si could stabilize it as the $Bi_{24}Si_2O_{40}$ phase at lower temperatures [39]. Furthermore, the same Raman peaks are observed in the case of $Bi_{24}Si_2O_{40}$ single crystal [39]. Therefore, it is very probable that the new phase observed was $Bi_{24}Si_2O_{40}$ [Paper I].

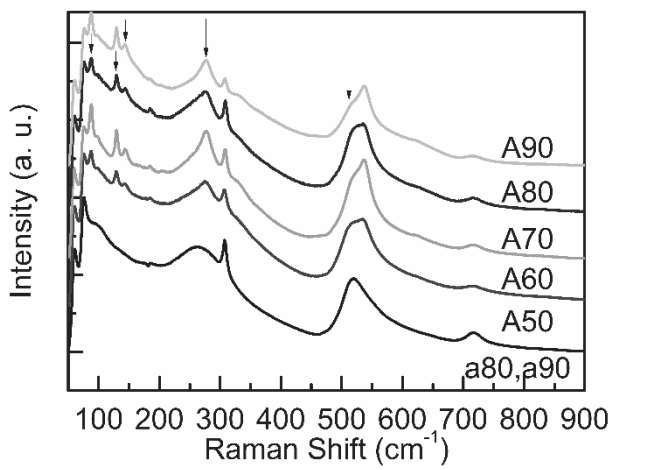

Fig. 8. Raman spectra of *x* wt% BBSZ – (100-*x*) wt% $BaTiO_3$ from *x* = 50-90 sintered at 400 °C and 450 °C (Paper I, published by permission of Elsevier).

Two different phases, $BaTiO_3$ and BBSZ glass, were observed in the backscattered electron image (Fig. 9(a)) of a90 sample sintered at 400 °C. This had a dense microstructure with low porosity. However, the microstructure of A60 and A70 samples in Fig. 9(b) and Fig. 9(c) revealed diversified characteristics and the existence of a new phase. The energy dispersive spectrometer (EDS) analysis verifies the dark grey areas as $BaTiO_3$ phase, the light grey as the BBSZ glass, and the white small areas as $Bi_{24}Si_2O_{40}$ phase. A60 and A70 both exhibited dense microstructure and similar size of the $Bi_{24}Si_2O_{40}$ phase around 200 nm while the voids (black colour) with sizes around 1-2 µm are shown in Fig. 9(b) of A60 sample. Despite the relatively low bulk density of the A60 sample, characteristics of dense microstructure were observed in small areas regardless of the voids. Fig. 9(b) indicates that the densification process at 450 °C of the A60 sample was proceeding, but was not completed. The possible reason is thought to be that the rearrangement mechanism of liquid sintering activates the densification and the capillary force exerted by the wetting liquid pulls the grains together. This is especially important for smaller particles. However, the next solid-precipitation mechanism has not yet been started. It indicates a low sample density but a dense microstructure with high liquid content [40]. Fig. 9(c) reveals that the cross-section surfaces of A70-A90 samples had dense and pore-less microstructures. Furthermore, Choi *et al.* [41]

reported that a small amount of Si could exist along the grain boundary composed of a Bi-rich phase. He *et al.* [42] also reported the precipitation of $Bi_{24}B_2O_{39}$ phase in a very similar glass, Bi_2O_3-B_2O_3-ZnO, at 460 °C. This corresponds to the backscattered images, XRD and Raman results of A60 and A70. All results confirm the existence of a $Bi_{24}Si_2O_{40}$ phase. Therefore, the likely reason that the bulk densities of the A80 and A90 samples were larger than the theoretical value was due to the higher density of the formed $Bi_{24}Si_2O_{40}$ phase (9.19 g/cm^3) [43].

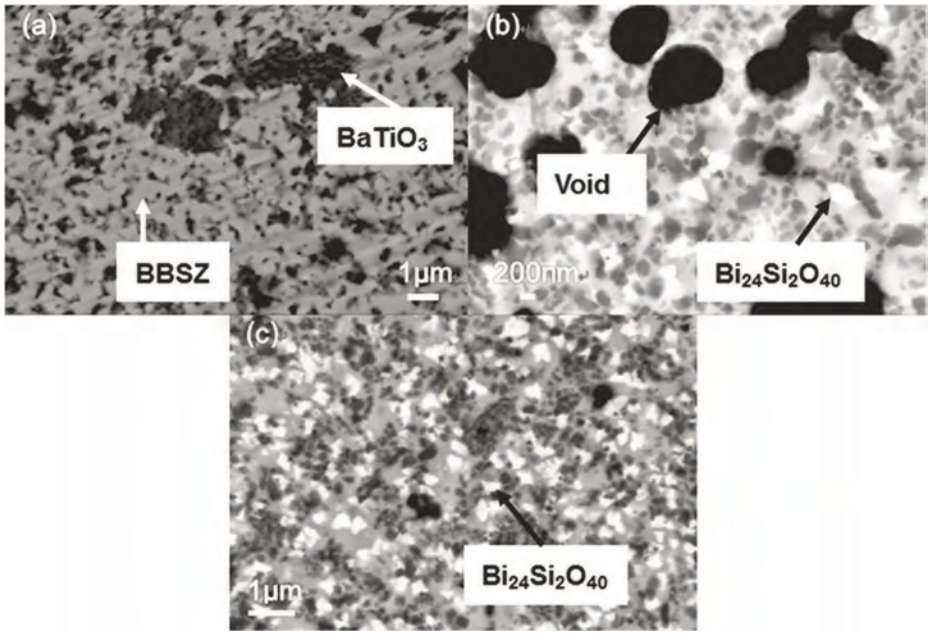

Fig. 9. Backscattered electron images of (a) a90 (sintered at 400 °C), and (b) A60 and (c) A70 sintered at 450 °C (Paper I, published by permission of Elsevier).

The dielectric properties of $BaTiO_3$–BBSZ composition sintered at 400 °C and 450 °C are illustrated in Table 3. The dielectric properties of the samples depend on the bulk densities, microstructures and dielectric properties of each phase. The bulk $BaTiO_3$ ceramics, sintered at 1350 °C for 2 hrs, had good dielectric properties (ε_r =1781, tan δ = 0.003 at 100 kHz, and ε_r = 3000 tan δ = 0.12 at 100 MHz). In the case of A80, a80 and A90, a90 samples, which had the same composition but a different sintering temperature, A80 and A90 samples had higher ε_r values than those of a80 and a90 due to the higher sintering temperature. However, the reason for the better dielectric properties of the A80 and A90 samples cannot only be

attributed to their bulk density and microstructure properties. The presence of the new phase plays an important role in their dielectric properties. Some references [4, 43-44, 46] reported ε_r values for $Bi_{24}Si_2O_{40}$ ceramic and single crystal of 37.6 - 56, respectively. Thus, the higher ε_r value of A80 and A90 may be attributed to the higher ε_r of the $Bi_{24}Si_2O_{40}$ phase compared to that of BBSZ glass. In the A60 samples, although the $Bi_{24}Si_2O_{40}$ phase exists, the low densities and high porosity could be a reason for the small ε_r values. Attention has been drawn to the smaller ε_r value of the A60 sample compared to that of the A50 sample. This is assumed to be due to the effect of the voids with 1-2 μm size which are shown in Fig. 9(b). The A70 sample exhibited the highest ε_r values of 132 and 207 with tan δ of 0.006 and 0.028 at 100 kHz and for 100 MHz, respectively. However, with glass concentrations over 70 wt%, the ε_r value reduced to 75.8 and 42.9 for the A80 and A90 samples at 100 kHz. The decline of the ε_r value is a result of the more dominant ε_r contribution from the BBSZ glass compared to that of $BaTiO_3$. The loss properties of the different samples at 100 kHz showed consistent values which were quite close to the loss of pure BBSZ glass (0.005). Additionally, Table 3 also shows that all ε_r values of different specimens at 100 MHz were higher than those at 100 kHz. It should further be noted that losses of A90 and a90 samples were even lower those of $BaTiO_3$ and BBSZ glass. The possible reasons could again be attributed to the existence of secondary phase $Bi_{24}Si_2O_{40}$ [Paper I].

Table 3. Dielectric properties of BBSZ-$BaTiO_3$ samples with different amounts of glass and different sintering temperatures (Paper I, published by permission of Elsevier).

	Sintering temperature	450 °C					400 °C	
	Sample	A50	A60	A70	A80	A90	a80	a90
	BBSZ(wt%):	50	60	70	80	90	80	90
	$BaTiO_3$(wt%):	50	40	30	20	10	20	10
ε_r	100 kHz	93.7	80.9	132	75.8	42.9	31.7	23.8
	100 MHz	136	121	207	115	63	43	36
tan δ	100 kHz	0.0045	0.0056	0.006	0.006	0.006	0.027	0.016
	100 MHz	0.020	0.020	0.028	0.014	0.011	0.010	0.007

3.3 Al_2O_3-BBSZ composites

The densification, microstructure and dielectric properties of the composites of BBSZ glass with 10-50 vol% Al_2O_3 filler were studied and discussed in Paper II.

Table 4 lists the true densities, bulk densities, relative densities and the porosity of BBSZ glass composites with 10-50 vol% Al_2O_3 which were sintered at 450 °C. The density of Al_2O_3 according to the data sheet is 3.97 g/cm^3 while the true density of BBSZ powder is 6.85 g/cm^3. As shown in Table 4, with more than 30 vol% addition of Al_2O_3 the sintered density decreased because the porosity increased. The samples with 20 vol% or 10 vol% of Al_2O_3 had low porosity (< 10%) and high relative density values [Paper II].

Table 4. Density and porosity of the composites with different amounts of Al_2O_3 sintered at 450 °C (Paper II, published by permission of John Wiley and Sons).

Al_2O_3 (vol%)	10	20	30	40	50
Bulk Density (g/cm^3)	6.55	6.35	5.08	3.73	3.20
True Density (g/cm^3)	7.02	6.92	6.03	5.63	4.95
Relative Density (%)	93	92	84	66	65
Porosity	0.07	0.08	0.16	0.34	0.35

Fig. 10 clearly shows the XRD patterns of BBSZ glass with different additions of Al_2O_3. The peaks related to the α-phase Al_2O_3 structure (dashed lines) and the increasing intensity of the broad background hump with θ values in the range of 20-35 ° is observed with increasing amounts of amorphous BBSZ glass. The extra peaks in Fig. 10 imply the existence of at least one unknown phase (denoted with X). The intensities of these peaks increased as the amount of Al_2O_3 was decreased. The best correlations to the unknown peaks were obtained with Bi_2O_3 or $Bi_{24}Si_2O_{40}$. Following the previous discussion of similar $BaTiO_3$-BBSZ compositions, these extra peaks were attributed to $Bi_{24}Si_2O_{40}$ phase [Paper II].

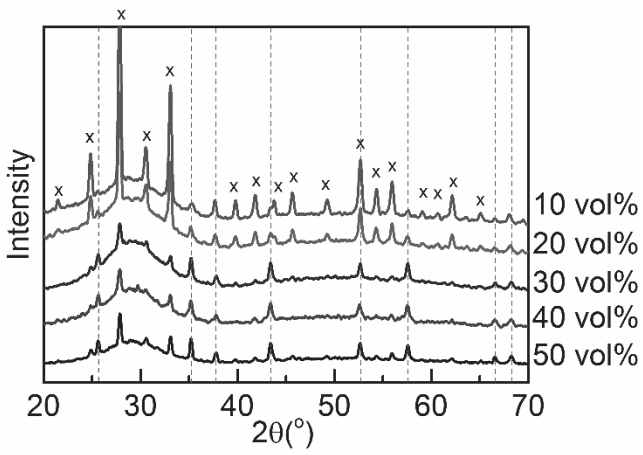

Fig. 10. XRD pattern of the composites with different vol% amounts of Al_2O_3 sintered at 450 °C. Dashed lines indicate the peaks of α–Al_2O_3 phase; the other peaks (denoted with X) corresponded to Bi_2O_3 (PDF 74-1375) or $Bi_{24}Si_2O_{40}$ (PDF 80-0627) (Paper II, published by permission of John Wiley and Sons).

Raman spectra of the BBSZ-Al_2O_3 composites are illustrated in Fig. 11. All of the Raman peaks belonging to Al_2O_3 phase are very weak, even the strongest one at 418 cm^{-1}, since its scattering level is low, as generally reported [45]. There are two peaks at 277 cm^{-1} and 537 cm^{-1}, marked with arrows in Fig. 11, which were also observed in the Raman spectra of $BaTiO_3$-BBSZ composites (Fig. 8) and in those measured for pure BBSZ. Nevertheless, the peaks below 150 cm^{-1} become more and more obvious with decreasing amounts of Al_2O_3. Thus, the Raman spectra provide more evidence to support the XRD results. The second $Bi_{24}Si_2O_{40}$ phase is generated in Al_2O_3-BBSZ composition sintered at 450 °C, which is identical to the results of the $BaTiO_3$-BBSZ composites.

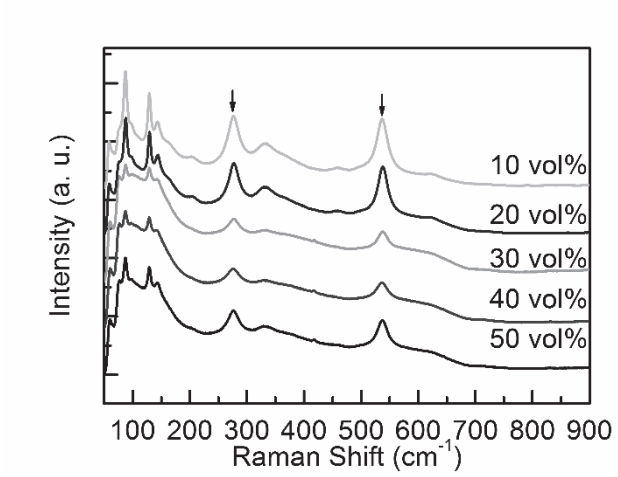

Fig. 11. Raman spectra of the BBSZ-Al_2O_3 composites with different amounts of Al_2O_3 sintered at 450 °C (Paper II, published by permission of John Wiley and Sons).

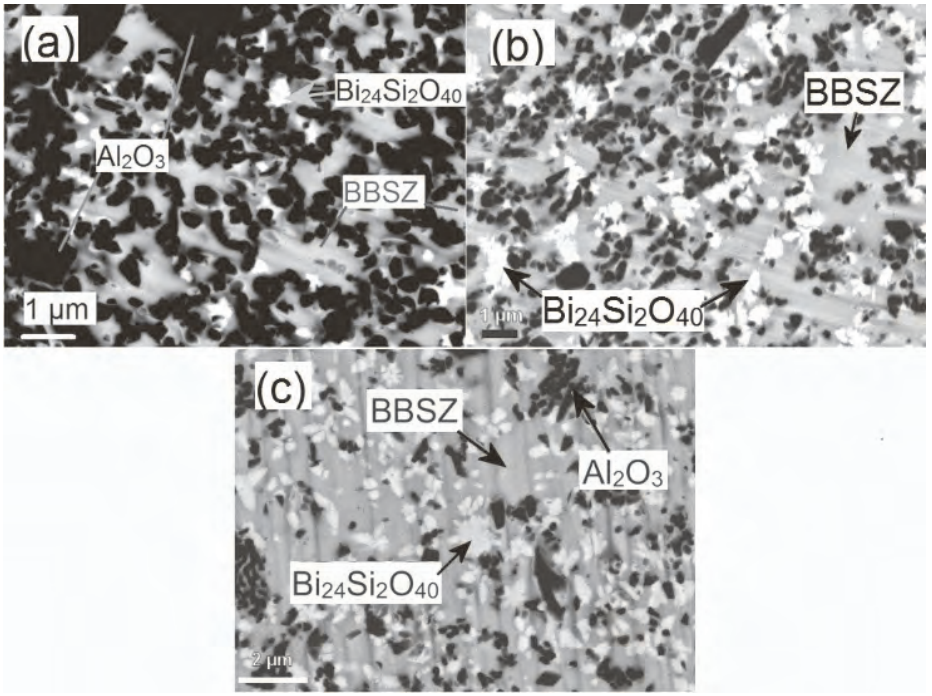

Fig. 12. Backscattered electron images of the composites with (a) 30 vol% and (b) 20 vol% and (c) 10 vol% addition of Al_2O_3 sintered at 450 °C (Paper II, published by permission of John Wiley and Sons).

Fig. 12 illustrates three different phases in the backscattered electron image of B70-B90. The EDS analysis reveals that the dark areas in Fig. 12 represent the Al_2O_3 phase, the light grey the BBSZ glass, and those with the bright white colour were denoted as $Bi_{24}Si_2O_{40}$ phase. The higher the Al_2O_3 content, the less the amount of $Bi_{24}Si_2O_{40}$ phase was observed [Paper II].

Table 5. Dielectric properties of the composites with different amounts of Al_2O_3 sintered at 450 °C (Paper II, published by permission of John Wiley and Sons).

Al_2O_3 (vol%)		10	20	30	40	50
ε_r	100 kHz	22.0	19.5	14.8	10.7	8.0
	100 MHz	31.4	27.7	20.8	12.6	8.4
	1 GHz	32.5	28.8	21.8	12.8	8.5
tan δ	100 kHz	0.006	0.004	0.004	0.005	0.004
	100 MHz	0.011	0.008	0.006	0.005	0.005
	1 GHz	0.019	0.009	0.016	0.010	0.008

The dielectric properties of the composites with different amounts of Al_2O_3 at 100 kHz, 100 MHz and 1 GHz are summarized in Table 5. Due to the limitation of measurements, the accuracy of the measured tan δ value is not high when the frequency approaches the GHz region. With higher amount of Al_2O_3, composites had a low relative permittivity due to porosity and the properties of pure Al_2O_3 (ε_r = 9.8-10.1 and tan δ = 0.00004-0.0002 at 1 MHz) [32], while the measured dielectric properties of the sintered pure BBSZ glass had much higher ε_r (~ 28 for 100 kHz, ~ 42 for 100 MHz, ~ 46 for 1 GHz). When a dense microstructure was achieved, the relative permittivity increased with decreasing amounts of Al_2O_3 and increasing frequency. The highest ε_r value reached was 32.5 at 1 GHz with 10 vol% addition of Al_2O_3. It is worth noting that all samples at 100 kHz had a dielectric loss value ~ 0.005, close to the tan δ value of pure BBSZ, but the tan δ gradually increased at 100 MHz and 1 GHz from 0.006 and 0.016 (30 vol% of Al_2O_3) to 0.011 and 0.019 (10 vol% of Al_2O_3). In order to determine the reasons for the higher loss at high frequency, a full understanding of the dielectric properties of $Bi_{24}Si_2O_{40}$ phase is needed, because the amount of $Bi_{24}Si_2O_{40}$ increased with decreasing additions of Al_2O_3, as shown in the XRD, Raman and FESEM analyses [Paper II].

Only a few researchers have discussed the dielectric behaviour of $Bi_{24}Si_2O_{40}$. Suvorov [4] reported that $Bi_{12}SiO_{20}$ ceramic sintered at 850 °C had the best dielectric properties (ε_r = 37.6, Qxf = 8 100 GHz at 5.5 GHz) among a series of sillienite compounds. Aldrich *et al.* [46] and Reddy [44] reported the dielectric behaviour of $Bi_{24}Si_2O_{40}$ single crystal. The ε_r and tan δ curves over 1 kHz to 100 kHz were quite flat. The evaluated ε_r and tan δ values at 100 kHz and 10 MHz were 50 and 46 and 0.013 and 0.0007, respectively.

Thus the dielectric behaviour of composites can be clearly described. When the amount of Al_2O_3 with low relative permittivity is decreased, the BBSZ and $Bi_{24}Si_2O_{40}$ phases with higher relative permittivity play a more prominent role in the dielectric properties, hence the ε_r increases at all frequencies. In addition, the losses of composites are affected by these three phases but in different manners. At 100 MHz and 1 GHz, the low loss values are attributed to the low tan δ of $Bi_{24}Si_2O_{40}$ and Al_2O_3. However, at 100 kHz the tan δ of $Bi_{24}Si_2O_{40}$ (0.013) is close to the measured loss value for the pure BBSZ glass while the low loss from the Al_2O_3 contribution is insignificant due to its low value [Paper II].

In short, the compositions of $BaTiO_3$ and Al_2O_3 based on the BBSZ glass matrix may be successfully fabricated in the ultra-low temperature region. The proposed $BaTiO_3$-BBSZ composites showed much higher ε_r values than those reported earlier. Also, the Al_2O_3-BBSZ composites performed with moderate

adjustable ε_r values and relatively low losses characteristics. They not only offer more potential applications, but also a lower sintering temperature. Compared with other research into ULTCC materials, $Bi_2Mo_2O_9$ thick films printed on Al foil sintered at 645 ^oC [10] have a larger relative permittivity and similar loss value (ε_r ~ 38, tan δ ~ 0.007 at 100 kHz) to Al_2O_3-BBSZ composites (ε_r ~ 8-22, tan δ ~ 0.004-0.006 at 100 kHz). But $BaTiO_3$-BBSZ composites exhibit high permittivity values and offer a significant advantage for multilayer capacitor applications. Furthermore, a glass ceramic of zinc borate $3ZnO–2B_2O_3$ (3Z2B) glass with 15 wt% SiO_2 filler composites [19] can be sintered at 650 ^oC for 0.5 hr and shows a much smaller loss value (~ 0.0013 at 1 MHz) and smaller ε_r (6.1 at 1 MHz) than Al_2O_3-BBSZ samples. However, the composites in this study had a much lower sintering temperature and a wide region of relative permittivity and acceptable loss values depending on the selection and amount of fillers for different ranges of frequency.

For most general cases, too high an amount of glass addition would ruin the original structures or produce a secondary phase that degrades the dielectric performance, despite the addition of glass being beneficial in obtaining a lower sintering temperature. However, the results with $BaTiO_3$-BBSZ and Al_2O_3-BBSZ compositions markedly indicate that not only a lower sintering temperature was achieved but also the degradation due to glass addition can be avoided. This is especially true if a suitable glass can be chosen and applied.

3.4 Different preparation effects on $BaTiO_3$-BBSZ glass ceramics

The thermal behaviour and dielectric properties of 50 wt% $BaTiO_3$- 50 wt% BBSZ composite with different treatments are discussed in Paper III.

There are several common methods to reduce sintering temperatures for ceramics, such as enlarging the surface area of particles, glass coating, and addition of fluoride [14-15]. In this study, the research related to the thermal behaviour of the 50 wt% $BaTiO_3$- 50 wt% BBSZ glass-ceramic composites with different glass particle sizes and LiF additions was conducted for a deeper understanding of the process at higher temperatures.

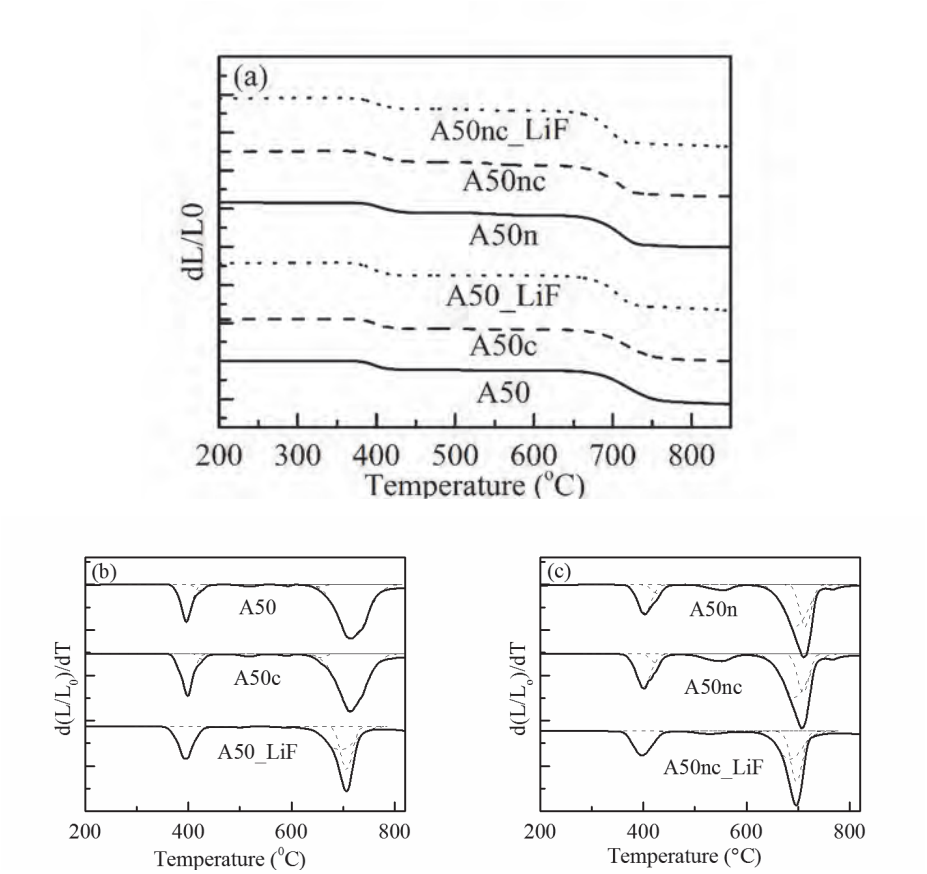

Fig. 13. (a) Dilatometric curves of 50 wt% $BaTiO_3$-50 wt% BBSZ glass composite with different procedure, (b) (c) and their derivation curves which were analyzed by Gaussian peaks (Paper III, published by permission of Elsevier).

As shown in Fig. 6, the composite of 50 wt% $BaTiO_3$-50 wt% BBSZ sintered at 450 °C had low density and high porosity. In addition, Fig. 5 also provides the dilatometric curve of this composite from room temperature to 550 °C. In this section, dilatometric experiments are performed not only to obtain a suitable sintering temperature for 50 wt% $BaTiO_3$-50 wt% BBSZ composite, but also to investigate the interactions between the glass and $BaTiO_3$ separately. The curves in Fig. 13(a) reveal the shrinkage behaviour of the composite with different treatments. These treatments are depicted in Fig. 1. The A50 sample denotes a sample with common size glass particles, A50n a sample with small glass particles, A50_LiF a

sample with common size glass particles with LiF addition, A50c with common size particles preheated at 390 °C, A50nc a sample with small glass particles preheated at 390 °C, and A50nc_LiF being as the previous one but with LiF addition.

There are two marked shrinkages observed at around 400 °C and 700 °C in the derivations of the dilatometric curves (Fig. 13(b)). The first shrinkage around 400 °C is a result of the softening and rearrangement of the glass particles, which is in line with the DSC results of BBSZ glass in Fig. 2. Almost full densification of the samples is achieved when the heating temperature rises to 720 °C. In addition, somewhat different shrinkage behaviour of different $BaTiO_3$-BBSZ composites is detected. The shrinkage of A50 sample shows a typical conventional process with two peaks at 400 and 422 °C, and a stronger one at 718 °C.

Table 6. Analyses of dilatometric curves (onset point) and their differential values (peaks) (Paper III, published by permission of Elsevier).

samples	onset point	peak position	peak position	onset	peak position	peak position
A50	388 °C	396 °C	422 °C	687 °C	NA	718 °C
A50c	383 °C	397 °C	426 °C	682 °C	NA	716 °C
A50_LiF	377 °C	395 °C	NA	685 °C	694 °C	706 °C
A50n	385 °C	402 °C	427 °C	679 °C	695 °C	714 °C
A50nc	382 °C	400 °C	425 °C	675 °C	693 °C	710 °C
A50nc_LiF	376 °C	399 °C	NA	673 °C	684 °C	697 °C

Table 6 summarizes the onset and maximum value of shrinkage rate of these six specimens. In Fig. 13(b), the A50 and A50c samples present similar peak shapes. The detectable intensity peak at 427 °C, relating to the amount of the secondary phase $Bi_{24}Si_2O_{40}$, is observed in both samples. The lower onset temperature of the A50c sample indicates that the pre-heating is beneficial to the sintering process and triggers the process a little earlier due to the lower surface tension, but it does not lower the sintering temperature or change the sintering mechanism. Additionally, the small size glass particles are expected to surround the $BaTiO_3$ particles more uniformly, to decrease the distance between the $BaTiO_3$ particles, and enhance the capillary pressure. However, the sintering temperature of composites with small glass particles shows only a slight decrease compared to those with the conventional process.

The A50, A50c, A50_LiF, and A50n, A50nc, A50nc_LiF samples sintered at 720 °C for 5 hrs had high density (~ 6.0 g/cm^3) with low porosity (< 2%). The XRD patterns of $BaTiO_3$-BBSZ composites sintered at 720 °C are shown in Fig. 14. A

Co target was used for the composites sintered at 720 °C in order to obtain higher accuracy. $BaBi_4Ti_4O_{15}$, $Bi_{24}Si_2O_{40}$ and zincate ZnO phase were seen in all six samples while pure BBSZ glass heated at 720 °C showed the existence of zinc silicate (Zn_2SiO_4) phase. Also, a very small amount of barium zinc silicate $BaZn(SiO_4)$ was observed in the samples with smaller glass size and LiF addition. Additionally, the intensities of the $Bi_{24}Si_2O_{40}$ and $BaBi_4Ti_4O_{15}$ phases greatly increased due to the LiF addition. At 720 °C the LiF addition not only enhances the generation of the secondary phases, but also decreases the sintering temperatures to some extent (Table 6). Induja et al. reported that the same BBSZ glass composition with 40 wt% Al_2O_3 sintered at 850 °C shows the $Bi_{24}Si_2O_{40}$ and $ZnAl_2O_4$ phase [47]. A similar silicate second phase of $Ba_2TiSi_2O_8$ is also found in $BaO\text{-}B_2O_3\text{-}SiO_2/BaTiO_3$ [48] and in the $ZnO\text{-}B_2O_3\text{-}SiO_2/BaTiO_3$ glass ceramic system [49]. Therefore, the interaction between glass and filler is hard to avoid at high heating temperatures (>700 °C).

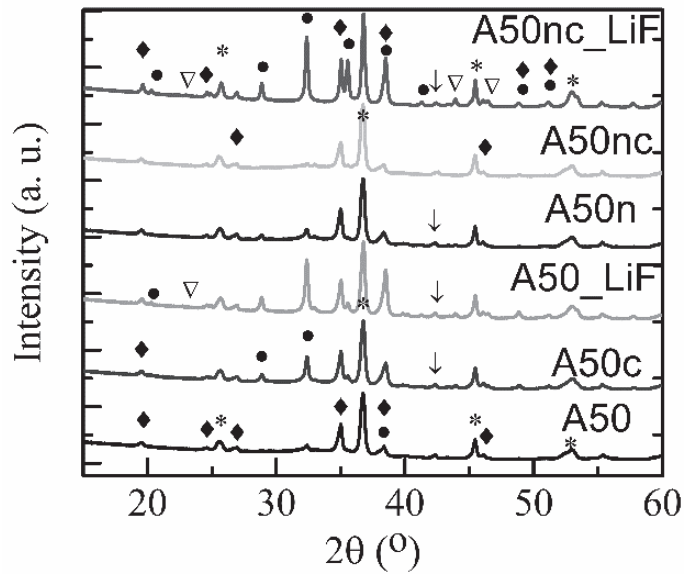

Fig. 14. XRD patterns of samples which were sintered at 720 °C (* refers to $BaTiO_3$, ● refers to $Bi_{24}Si2O_{40}$, ♦ refers to $BaBi_4Ti_4O_{15}$) (Paper III, published by permission of Elsevier).

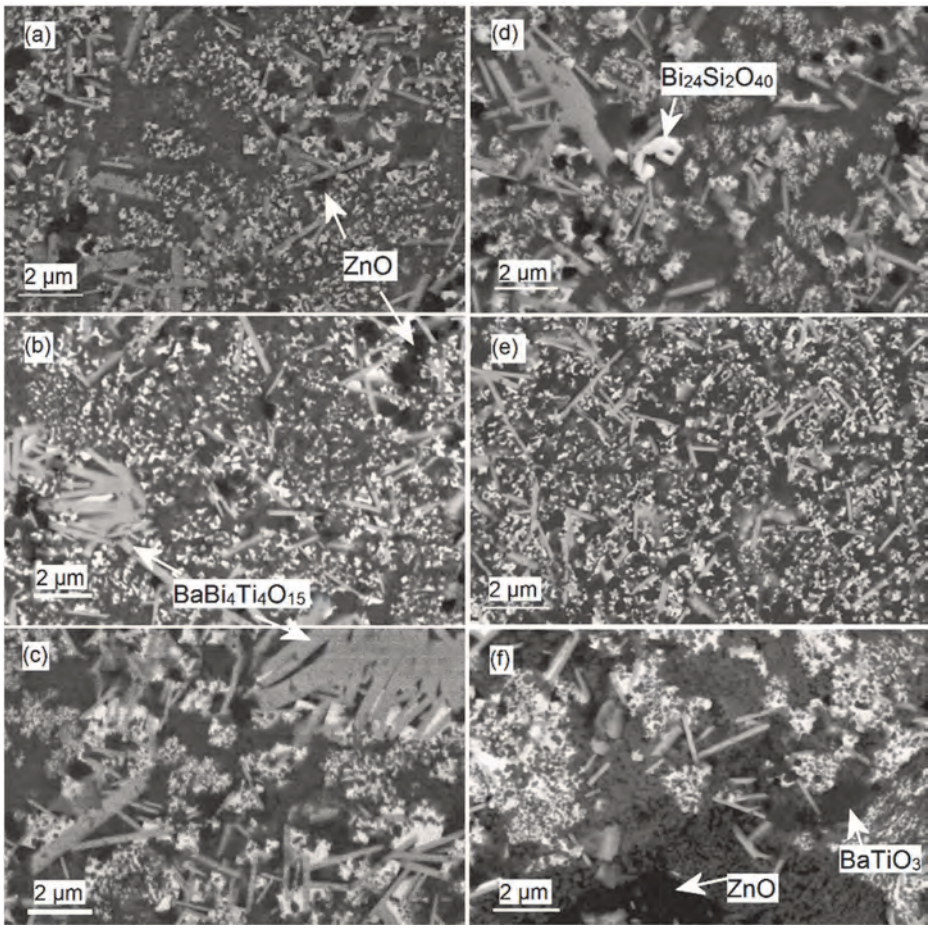

Fig. 15. (a) Backscattered electron images of A50 and (b) A50c (c) A50_LiF, (d) A50n, (e) A50nc, and (f) A50nc_LiF samples sintered at 720 °C for 5 hrs. Black areas refer to ZnO, dark grey $BaTiO_3$, light grey $BaBi_4Ti_4O_{15}$ and the bright ones to $Bi_{24}Si_2O_{40}$ (Paper III, published by permission of Elsevier).

The backscattering electron images of different samples in Fig. 15 clearly show the different phases and microstructures of samples with ZnO (black areas), $BaTiO_3$ phase (dark grey), $Bi_4BaTi_4O_{15}$ phase (light grey rod-shape), and $Bi_{24}Si_2O_{40}$ phase (bright white). Fig. 15(c) and Fig. 15(f)) show that the samples with LiF addition clearly had higher amounts of $Bi_4BaTi_4O_{15}$ and $Bi_{24}Si_2O_{40}$. This is in good agreement with the XRD results. The formation of large clusters of ZnO phase is clearly shown in Fig. 15(f) for all of samples except for the A50nc sample. Fig. 15(e) shows the small size of different phases homogenously distributed in the

dense structures. This indicates that the small particle size, together with the pre-heating process for coating at 390 °C, inhibited the clustering of particles with different phases.

Table 7. Dielectric properties of A50, A50n, and A50_LiF sintered 720 °C (Paper III, published by permission of Elsevier).

Sintered 720 °C @100 kHz	ε_r	tan δ
A50	255	0.013±0.001
A50c	248	0.013±0.001
A50_LiF	202	0.017±0.001
A50n	259	0.013±0.001
A50nc	248	0.013±0.001
A50nc_LiF	186	0.018±0.001

Table 7 contains the dielectric properties at 100 kHz of six samples sintered at 720 °C for 5 hrs. A50, with a different glass particle size and coating process, had a relatively high ε_r of 248 - 259 with the same tan δ of 0.013, while the small LiF addition in the A50 and A50nc samples decreased the ε_r to 186-211 and increased the loss value to 0.017-0.018. The smaller relative permittivity and higher loss of the A50_LiF can be influenced to the second phase contributions, which can be observed in the microstructure and XRD results. As detailed in the earlier discussion, the dielectric properties are dominated by the bulk density, phase characteristics, and microstructure. Almost full densification was achieved for all samples sintered at 720 °C. Thus, the characteristics and contributions of each phase play the dominant role. As noted in Section 3.2, $Bi_{24}Si_2O_{40}$ shows a low ε_r value (~ 46) and tan δ (~ 0.005) at 1 MHz, and bulk $BaTiO_3$ has a high ε_r (~ 1781) and tan δ of (~ 0.003) at 100 kHz. However, the dielectric properties of the $BaBi_4Ti_4O_{15}$ are difficult to determine due to its highly anisotropic structure. The relative permittivity of the ab- and c-axes for $BaBi_4Ti_4O_{15}$ phase has been reported to be 1000 and 110 at 1 kHz, respectively [50]. Also, other relative permittivity values have been reported [50-53]. The relative permittivity decreased with the increased amount of $BaBi_4Ti_4O_{15}$ phase, which is due to the decreasing amount of high ε_r $BaTiO_3$ phase. Furthermore, the tan δ for $BaTiO_3$ is ~ 0.003 at 100 kHz, and for $Bi_{24}Si_2O_{40}$ ~ 0.005 at 1 MHz [11], but the measured loss of the samples was higher than the values of these two phases. It can be assumed that the $BaBi_4Ti_4O_{15}$ phase is responsible for the high loss values, especially in the case of the samples with LiF addition. The tan δ for the $BaBi_4Ti_4O_{15}$ as measured by Cui *et al.* [52] was ~ 0.0135 at 1 kHz and by Diao *et al.* [53] ~ 0.025 at 1 MHz. It has been also reported

that in these kinds of Aurivillius perovskite composites the high losses are associated with their ferroelectric properties [50-53].

The effect of different treatments on 50 wt% $BaTiO_3$-50 wt% BBSZ composite has been studied. Above the crystallization temperature of glass, the active reactions between $BaTiO_3$ and BBSZ glass were investigated. $BaBi_4Ti_4O_{15}$ phase was observed in $BaTiO_3$-BBSZ composites sintered at 720 ^oC. The achieved microstructures were very dense and dielectric properties suitable for some miniaturization and packaging applications such as embedded capacitors where high relative permittivity is needed. Furthermore, it is also practicable to co-fire with materials having a similar sintering temperature but much lower relative permittivity, such as $Li_3Al_2B_2O_6$ [54], $BaNd_2Ti_5O_{14}$+La_2O_3-B_2O_3-TiO_2 [55], and $TiTe_3O_8$ ceramic in the TiO_2-TeO_2 system [56].

Regarding the reactive BBSZ glass system at higher temperature (> 500 ^oC), it is supposed that Al_2O_3-BBSZ has a similar behaviour when the heating temperature rises to 700 ^oC. The $ZnAl_2O_4$ phase was found in the BBSZN glass system (22.7 Bi_2O_3-23.3 B_2O_3- 13.5SiO_2-37.9 ZnO-2.6 Na_2O for mol%) [57]. Furthermore, Induja *et al.* also reported the existence of $ZnAl_2O_4$ in composites of 40 wt% Al_2O_3-60 wt% BBSZ glass, which were sintered at 850 ^oC [47]. Thus, it is important to understand the thermal and crystallized behaviour of a glass before its utilization.

3.5 A practical application: multilayer structures with embedded electrodes

A feasible demonstration of the fabrication of multilayer structures using the 30 wt% $BaTiO_3$-70 wt% BBSZ and 30 vol% Al_2O_3-70 vol% BBSZ composites was performed. None of the well-known binder systems for LTCC [58], like the one based on PVB, are suitable for ULTCC due to their high burn-out temperature (~ 400 ^oC). Therefore, tape casting for ULTCCs with the sintering temperature approaching 500 ^oC has not been reported. In this thesis, a novel binder system is introduced in Table 1, which enables the reduction of the tape sintering temperatures to 300 ^oC. This can be observed in the TGA/DSC measurements in Fig. 16. The organic components in the green tapes were burned out at temperature of 250 ^oC with a heating rate of 2 ^oC/min and the specimen weight of 15.4 mg. Therefore, this organic system can be practically applied for various ULTCC materials, even those with sintering temperature close to 300 ^oC.

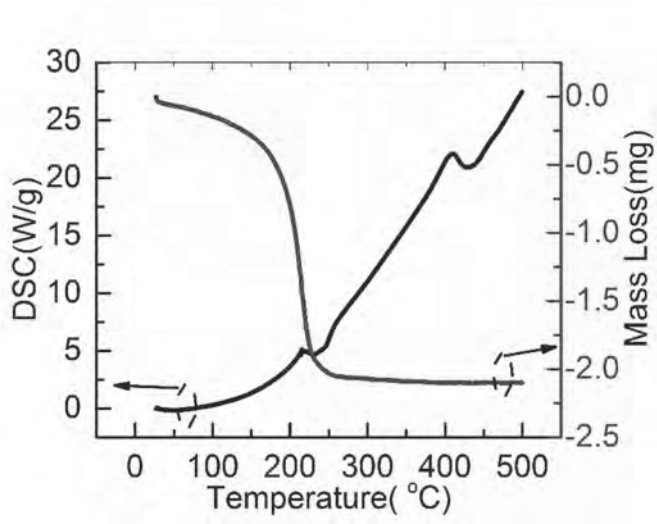

Fig. 16. Thermogravimetric analysis and differential scanning calorimetry (TGA/DSC) diagram of a green tape (Paper IV, published by permission of John Wiley and Sons).

A suitable sintering temperature can be determined to be the same temperature as that for $BaTiO_3$-BBSZ and Al_2O_3-BBSZ composites. According to the results, the sintering profile can be proposed as an increasing temperature with a 3 °C/min heating rate from room temperature to 250 °C, dwelling at 250 °C for 1 hr to burn out the organics completely, and then increasing the temperature to 450 °C with 1 °C/min heating rate, dwelling at 450 °C for 1 hr.

Table 8. Shrinkage rates of $BaTiO_3$-BBSZ, Al_2O_3-BBSZ and multimaterial stacks in x&y- and z-directions and volume shrinkage rates and bulk densities (Paper IV, published by permission of John Wiley and Sons).

Bulk Density of Sintered tape	Al_2O_3-BBSZ	$BaTiO_3$-BBSZ	Multilayers
x&y shrinkage rate (%)	26	24	25
z shrinkage rate (%)	28	29	31
Volume shrinkage rate (%)	61	59	62
Bulk density (g/cm^3)	5.62	5.97	5.76

Table 8 shows the linear and volume shrinkages and bulk density of $BaTiO_3$-BBSZ and Al_2O_3-BBSZ, and multimaterial stacks sintered at 450 °C for 1 hr. There was only 2% difference of shrinkage rates between the two composites. Also, there was no evidence of the formation of defects between different layers during sintering.

Both sintered modules exhibited high densities (Table 8), which were close to the values of the bulk sample (6.36 g/cm^3 for $BaTiO_3$-BBSZ and 5.08 g/cm^3 for Al_2O_3 -BBSZ). The density of the multimaterial module is also presented as the average of the density value of both tapes. In addition the shrinkage rates of the embedded and top electrodes are in the same level as for the tapes.

The backscattered electron images in Fig. 17 show dense microstructures for sintered modules which are similar to the phase structures of the sintered bulk samples in Fig. 9 and Fig. 12. Fig. 17(a) presents the microstructures of Al_2O_3-BBSZ tape and silver electrode co-fired at 450 ^oC, where no chemical reaction or diffusion may be detected. This is proven by the linear EDS analysis (inset figure). Furthermore, no diffusion or cracks were observed at the interface of the multimaterial stack (Fig. 17(b)).

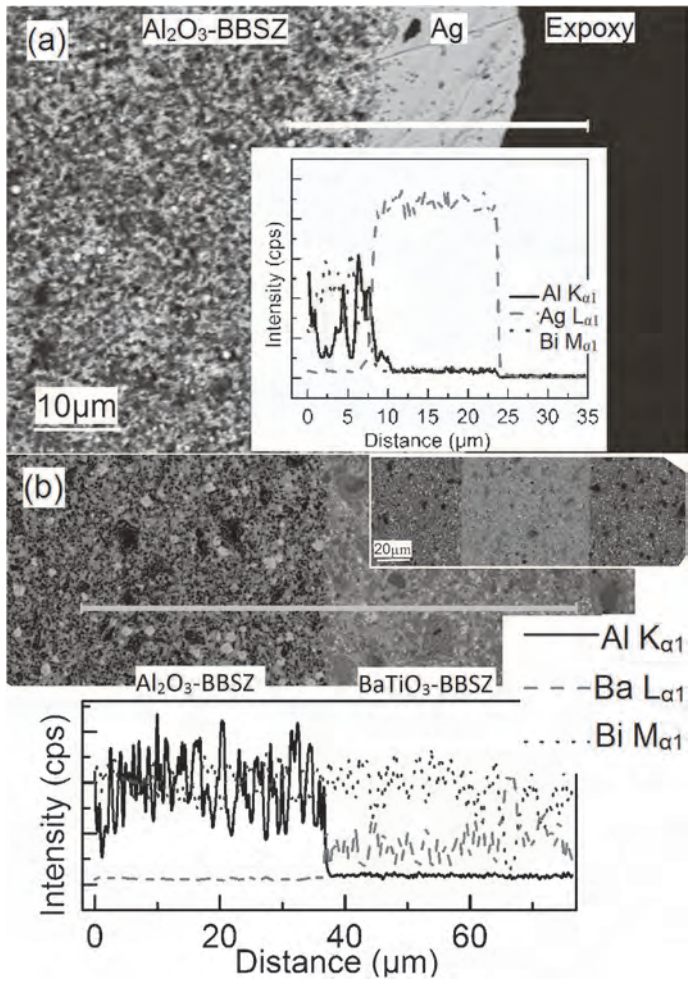

Fig. 17. (a) Backscattered electron image and linear EDS analysis of the Al_2O_3-BBSZ tape with sliver electrode and (b) multimaterial stacks after sintering at 450 °C for 1 hr with insert showing a 3-layers structure (Paper IV, published by permission of John Wiley and Sons).

4 Conclusion

The purpose of this thesis was to develop glass-ceramics composites based on BBSZ glass matrices with ultra-low sintering temperatures and to investigate their properties. Two glass ceramics compositions, *x* wt% $BaTiO_3$-(100-*x*) wt% BBSZ and *x* vol% Al_2O_3- (100-*x*) vol% BBSZ *x* = 10-50, were developed and the characteristics of composites were studied.

First of all, the properties of pure BBSZ provided the information for further study when developing related glass-ceramic composites. The transition temperature (T_g) and softening temperature (T_s) of the BBSZ glass are at around 382-386 ^oC and 416 ^oC, respectively. The particle size severely influenced the crystallization temperature; T_c of the glass is 483 ^oC for the BBSZ bulk, and 462 ^oC and 430 ^oC for the BBSZ and n-BBSZ powders, respectively. These results show that the reduced particle size markedly decreased its Tc. Also, the fluoride addition further assisted in lowering T_c of n-BBSZ to the value of 423 ^oC.

Regarding the $BaTiO_3$-BBSZ composite, dilatometric measurements with different glass content revealed that shrinkages started at about 382-386 ^oC, which corresponds to the transition temperature (T_g) of glass. The shrinkage rates increased with the amount of the glass. With a glass concentration of 70 wt% for $BaTiO_3$-BBSZ composites, a dense microstructures and useful dielectric properties were achieved at the ultra-low sintering temperatures of 400 ^oC and 450 ^oC. Density, Raman, XRD, and backscattered electron images measurements revealed that an additional phase $Bi_{24}Si_2O_{40}$ appeared after sintering at 450 ^oC, while only two initial phases ($BaTiO_3$, BBSZ glass) were observed in samples sintered at 400 ^oC. Moreover, the microstructure of the 60 wt% glass sample exhibited many 1-2 μm size voids. These voids originated from the capillary force and surface tension of the liquid, described as the rearrangement mechanism of the liquid phase sintering process. Additionally, these voids caused the small relative permittivity value, though a partly dense microstructure was obtained. 30 wt% $BaTiO_3$- 70 wt% BBSZ composite sintered at 450 ^oC showed high ε_r values of 132 and 207 at 100 kHz and 100 MHz, respectively. For the samples with 80 and 90 wt% of BBSZ glass addition, the dielectric ε_r values were reduced because of the high content of glass with low ε_r. Meanwhile, the loss properties of composites were dominated by the characteristics of glass, $BaTiO_3$, and $Bi_{24}S_{i2}O_{40}$ phase, especially for the samples with large amounts of glass (70 - 90 wt%). Actually, the existence of the secondary phase $Bi_{24}Si_2O_{40}$ may not hinder but enhance the dielectric properties.

The Al_2O_3-BBSZ composites showed features similar to those of the $BaTiO_3$-BBSZ. Not only the same densification behaviour, where high densification was achieved with 70 vol% glass content or higher, but also in microstructure and phase identification (Al_2O_3, BBSZ glass, and $Bi_{24}Si_2O_{40}$) in the samples. The relative permittivity increased with decreasing amounts of Al_2O_3, from 8.0 to 22 and 8.4 to 31.4 and 8.5 to 32.5 at 100 kHz, 100 MHz and 1 GHz, respectively. All the samples at 100 kHz showed tan $\delta \sim 0.005$, close to the tan δ value of pure BBSZ, but at 100 MHz and 1 GHz, tan δ gradually increased from 0.006 and 0.016 (30 vol% of Al_2O_3) to 0.011 and 0.019 (10 vol% of Al_2O_3). These dielectric results can be explained by the co-existence of the three phases, BBSZ glass, Al_2O_3 and $Bi_{24}Si_2O_{40}$.

However, the densification of samples with low glass content (< 70%) is poor for practical applications when sintered at 450 ^oC. The sintering dynamics mechanism and the effects of different thermal treatments on their microstructures and dielectric properties of 50 wt% $BaTiO_3$- 50 wt% BBSZ composite was investigated and discussed. Shrinkage at 400 ^oC and a larger shrinkage at around 700 ^oC which is associated with the $Bi_4BaTi_4O_{15}$ phase generation was observed. Dense but different microstructures and the existence of $Bi_4BaTi_4O_{15}$, $BaTiO_3$, and $Bi_{24}Si_2O_{40}$ phases were observed in the composite with different thermal treatments. The same dielectric properties (ε_r = 263-267, tan δ = 0.013 at 100 kHz) were obtained after sintering at 720 ^oC regardless of the size of the glass particles. The resulting rather high loss was thought to be attributed to the contribution of $Bi_4BaTi_4O_{15}$ phase. This was even more obvious in the case when LiF was added, since it increased the amount of $Bi_4BaTi_4O_{15}$. These samples did not meet the requirements for ULTCC material, but their achieved microstructures were dense and their dielectric properties were suitable for some miniaturization and packaging LTCC applications, such as embedded capacitors where high relative permittivity is needed, and for co-firing with other lower relative permittivity materials with a similar sintering temperature.

Finally, a practical demonstration of the fabrication of multilayer structures using the 30 wt% $BaTiO_3$- 70 wt% BBSZ and 30 vol% Al_2O_3-70 vol% BBSZ composites with a new binder system was introduced and performed using the tape casting method. The thermal analysis (DSC/TGA) of green tapes showed that the organic additives were burned out at temperatures around 250 ^oC. The composites of BBSZ glass with Al_2O_3 and $BaTiO_3$ fillers had differing relative permittivity values (14.8 and 132 at 100 kHz) but similar shrinkages and thus could be co-fired at 450 ^oC with silver electrodes without cracking and obvious diffusion.

To conclude all results, the glass-ceramic composites based on BBSZ glass not only enable sintering at ultra-low temperature (450 °C) but also fabrication of materials with a wide range of relative permittivity and acceptable loss using different fillers while the glass content is kept sufficient. In addition, by using a developed binder system for tape casting of ULTCCs, a multilayer module with $BaTiO_3$-BBSZ, Al_2O_3-BBSZ and embedded silver electrode may successfully be co-fired without observable cracks or diffusion. It can be expected that with the use of different fillers, such as ferroelectric, ferromagnetic, or ferrite materials, the composites will exhibit distinctive properties for various applications. Therefore, the developed glass-ceramics in this thesis have been clearly shown to be potential candidates for the further advancement of environmentally friendly ceramics sintered at ultra-low temperature. Furthermore, the multimaterial multilayers pattern sintered at ultra-lower temperature paves a new way for electroceramics to fabricate 3D electronics packages and high frequency devices with ultimate low fabrication costs based on the well-developed tape casting technique.

References

1. Sebastian MT (2008) Dielectric materials for wireless communication. Elsevier, Oxford: 1-10.
2. Sebastian MT, Jantunen H (2008) Low loss dielectric materials for LTCC applications: a review. Int Mater Rev 53: 57-90.
3. Sebastian MT, Wang H, Jantunen H (2016) Low temperature co-fired ceramics with ultra-low sintering temperature: a review. Curr Opin Solid State Mater Sci 20: 151-170.
4. Valant M, Suvorov D (2001) Processing and dielectric properties of sillenite compounds $Bi_{12}MO_{20-\delta}$ (M=Si, Ge, Ti, Pb, Mn, $B_{1/2}P_{1/2}$). J Am Ceram Soc 84: 2900-2904.
5. Zhou D, Randall CA, Wang H, Pang LX, Yao, X (2010) Microwave dielectric ceramics in Li_2O-Bi_2O_3-MoO_3 system with ultra-low sintering temperatures. J Am Ceram Soc 93: 1096-1100.
6. Zhou D, Randall CA, Pang LX, Wang H, Wu XG, Guo J, Zhang GQ, Shui L, Yao X (2001) Microwave dielectric properties of $Li_2(M^{2+})_2Mo_3O_{12}$ and $Li_3(M^{3+})Mo_3O_{12}$ (M = Zn, Ca, Al, and In) Lyonsite-related-type ceramics with ultra-low sintering temperatures. J Am Ceram Soc 94: 802−805.
7. Kwon D, Lanagan MT, Shrout TR (2007) Microwave dielectric properties of BaO-TeO_2 binary compound. Mater Lett 61: 1827-1831.
8. Wang SF, Wang YR, Hsu YF, Lu HC, Tsai JS (2010) Ultra-low-fire $Te_2(Mo1-_xW_x)O_7$ ceramics: microstructure and microwave dielectric properties. J Am Ceram Soc 93: 4071-4074.
9. Rödel J, Jo W, Seifert KTP, Anton E, Granzow T (2009) Perspective on the Development of Lead free Piezoceramics. J Am Ceram Soc 92: 1153-1177.
10. Liu W, Wang H, Zhou D, Li K (2010) Dielectric Properties of Low-Firing $Bi_2Mo_2O_9$ Thick Films Screen Printed on Al Foils and Alumina Substrates. J Am Ceram Soc 93: 2202–2206.
11. Zanotto ED (2010) A bright future for glass-ceramics. Am Ceram Soc Bull 89: 19-27.
12. Wang SF, Wang YR, Hsu YF, Chiang CC (2010) Densification and microwave dielectric behaviors of CaO-B_2O_3-SiO_2 glass-ceramics prepared from a binary glass composite. J Alloys Compd 498: 211-216.
13. Chiang CC, Wang SF, Wang YR, Hsu YF (2008) Characterization of CaO-B_2O_3-SiO_2 glass-ceramics: thermal and electrical properties. J Alloys Compd 461: 612-616.
14. Hsi CS, Chen YC, Jantunen H, Wu MJ, Lin TC (2008) Barium titanate based dielectric sintered with a two-stage process. J Euro Ceram Soc 28: 2581.
15. Hsi CS, Chen MY, Jantunen H, Hsi FC, Lin TC (2011) Sintering of titanate based dielectrics doped with lithium fluoride and calcium borosilicate glass. Mater Sci-Poland 29: 29-34.
16. Chen CS, Chou CC, Shih WJ, Liu KS, Chen CS, Lin IN (2003) Microwave dielectric properties of glass-ceramic composites for low temperature co-firable ceramics. Mater Chem Phys 79: 129-134.

17. Wu JM, Huang HL (1999) Microwave properties of zinc, barium and lead borosilicate glasses. J Non-Cryst Solids 260: 116-124.
18. Rahesh S, Jantunen H, Letz M, Willhelm SP (2012) Low temperature sintering and dielectric properties of alumina-filled glass composites for LTCC applications. Int J Appl Ceram Technol 9: 52-59.
19. Yu H, Liu J, Zhang W, Zhang (2015) Ultra-Low sintering temperature ceramics for LTCC applications: a review. J Mater Sci: Mater Eleectron 26: 9414-9423.
20. Honkamo J, Jantunen H, Subodh G, Sebastian MT, Mohanan P (2009) Tape casting and dielectric properties of $ZnTe_3O_8$-based ceramics with an ultra-low sintering temperature. Int J Appl Ceram Technol 6: 531-536.
21. Fajans K, Kreidl NJ (1948) Stability of lead glasses and polarization of ions. J Am Ceram Soc 31: 105-114.
22. Ermolenko NN, Manchenko ZF, Samujlova VN, Shamkalovich V (1980) Low-mleting glass. USSR Patent SU775061.
23. Ermolenko NN, Manchenko ZF, Karpovich EF, Tikhonv IA, Saevich NG, Panov LI, Sokolovskii BR (1985) Glass. USSR Patent SU1169951.
24. Maeder T (2012) Review of Bi_2O_3-based glasses for electronics and related applications. Int Mater Rev 58: 3-40.
25. Hasegawa S, Onishi H, Kanai M, Kamimoto T (2005) Bismuth glass composition, and magnetic head and plasma display panel including the same as sealing member. US Patent US2005-0181927A1.
26. Dyamant I, Itzhak D, Hormadaly J (2005) Thermal properties and glass formation in SiO_2-B_2O_3-Bi_2O_3-ZnO quaternary system. J Non-Cryst Solids 351: 3503-3507.
27. Dernovsek O, Naeini A, Preu G, Wersing W, Eberstein M, Schiller WA (2001) LTCC glass-ceramic composites for microwave application. J Euro Ceram Soc 21: 1693-1697.
28. Thomas S, Sebastian MT (2008) Effect of B_2O_3-Bi_2O_3-SiO_2-ZnO glass on the sintering and microwave dielectric properties of $0.83ZnAl_2O_4$-$0.17TiO_2$. Mater Res Bull 43: 843-851.
29. Hsiang H, Chen T (2009) Electrical properties of low-temperature-fired ferrite–dielectric composites. Ceram Int 35: 2035-2039.
30. Ling W, Zhang H, Li Y, Chen D, Wen Q, Shen J (2010) Effect of B_2O_3–Bi_2O_3–SiO_2–ZnO glass on the dielectric and magnetic properties of ferroelectric/ferromagnetic composite for low temperature cofired ceramic technology. J Appl Phys 107: 09D911.
31. Hsiang H, Chen T (2008) Dielectric and magnetic properties of low-temperature-fired ferrite-dielectric composites. J Am Ceram Soc 91: 2043–2046.
32. Moulson J and Herbert JM (2003) Electroceramics: Materials, Properties, Applications. England, John Wiley & Sons Ltd: 277.
33. Gao L, Hong JS, Miyamot H, Torre SDDL (2000) Bending strength and microstructure of Al_2O_3 ceramics densified by spark plasma sintering. J Eur Ceram Soc 20: 2149-2152
34. Goswami AK (1969) Dielectric properties of unsintered Barium Titanate. J Appl Phys 40: 619.

35. Choi Y, Park J, Ko W, Park J, Nahm S, Park J (2005) Low Temperature Sintering of $BaTi_4O_9$-Based Middle-k Dielectric Composition for LTCC Applications. J Electroceramics 14: 157-162.
36. Agilent Technologies Inc (2004) Agilent 4284A Precision LCR meter. 5963-5390E datasheet, USA, Sept 21.
37. Agilent Technologies Inc (2011) Agilent E4991A RF Impedance/Material Analyzer. 5980-1233E datasheet, USA, Jun. 13.
38. Salazar-Pérez AJ, Camacho-López MA, Morales-Luckie RA, Sánchez-Mendieta V, Ureña-Núñez F, Arenas-Alatorre J (2005) Structural evolution of Bi_2O_3 prepared by thermal oxidation of bismuth nano-particles. Superficies y Vacío 18: 4-8
39. Mihailova B, Gospodinov M, Konstantinova L (1999) Raman spectroscopy study of sillenites. I. Comparison between $Bi_{12}(Si,Mn)O_{20}$ single crystals. J Phys Chem Solids 60: 1821–1827.
40. German RM, Suri P, Park SJ (2009) Review: liquid phase sintering. J Mater Sci 44: 1-39.
41. Choi C, Ji M, Ko K, Shin J, Chang B, Sinn D (2004) Electrostatic Discharge (ESD) Reliability Improvement of ZnO-Bi based Multilayered Chip Varistor. CARTS Europe 2004: 18th annual passive components conference: 18-21.
42. He F, Cheng JS, Deng DW, Wang J (2010) Structure of Bi_2O_3-ZnO-B_2O_3 system low-melting sealing glass. J Cent South Univ Technol 17: 257-262.
43. Arizmendi L, Cabrera JM, Agullo-Lopez F (1992) Material properties and photorefractive behavior of BSO family crystals. Int J Optoelectron 7: 149-180.
44. Reddy YR, Sirdeshmukh L (1987) Dielectric Behaviour of $Bi_{12}SiO_{20}$. Phys Stat Sol (a) 103: K157.
45. Porto SPS, Krishnan RS (1967) Raman Effect of Corundum. J Chem Phys 47: 1009-1012.
46. Aldrich RE, Hou SL, Harvill ML (1971) Electrical and Optical Properties of $Bi_{12}SiO_{20}$. J Appl Phys 42: 493-494.
47. Induja IJ, Abhilash P, Arun S, Suredran KP, Sebastian MT (2015) LTCC tapes based on Al_2O_3–BBSZ glass with improved thermal conductivity. Ceram Int 41: 13572-13581.
48. Wang KT, He Y, Liang ZY, Cui XM (2015) Preparation of LTCC materials with adjustable permittivity based on BaO-B_2O_3-SiO_2/$BaTiO_3$ system. Mater Res Bull 65: 249-252.
49. Hsiang HI, Hsi CS, Huang CC, Fu SL (2008) Sintering behavior and dielectric properties of $BaTiO_3$ ceramics with glass addition for internal capacitor of LTCC. J Alloys Compd 459: 307-310.
50. Jardiel T, Caballero AC, Villegas M (2008) Aurivillus cearmics: $Bi_4Ti_3O_{12}$-based piezoelectrics. J Ceram Soc Jpn 116: 511-518.
51. Bobic JD, Petrovic MMV, Stojanovic BD (2013) Aurivillius $BaBi_4Ti_4O_{15}$ based compound: Structure, synthesis and properties. Processing and Application of ceramics 7: 97-110.
52. Cui Y, Fu X, Yan K (2012) Effects of Mn-Doping on the Properties of $BaBi_4Ti_4O_{15}$ Bismuth Layer Structured Ceramics. J Inorg Organomet Polym 22: 82-85.

53. Diao CL, Xu JB, Zheng HW, Fang L, Gu YZ, Zhang WF (2013) Dielectric and piezoelectric properties of cerium modified $BaBi_4Ti_4O_{15}$ ceramics. Ceram Int 39: 6991-6995.
54. Ohsahi M, Ogawa, H, Kan A, Tanaka E (2005) Microwave dielectric properties of low-temperature sintered $Li_3AlB_2O_6$ ceramic. J Euro Ceram Soc 25: 2877-2881.
55. Jung BH, Hwang SJ, Kim HS (2005) Glass-ceramic for low temperature co-fired dielectric ceramic materials based on La_2O_3-B_2O_3-TiO_2 glass with BNT ceramics. J Euro Ceram Soc 25: 3187-3193.
56. Udovic M, Valant M, Suvorov D (2001) Dielectric characterization of ceramics from the TiO_2-TeO_2 system. J Euro Ceram Soc 21: 1735-1738.
57. Kim KS, Shim SH, Kim S, Yoon SO (2010) Microwave dielectric properties of ceramic/glass composites with bismuth-zinc borosilicate glass. J Ceram Proc Res 11: 47-51.
58. Sebastian MT, Jantunen H (2015) Low-loss dielectric ceramic materials and their properties. Int Mater Rev 60: 392-412.

Original publications

I Chen Mei-Yu, Juuti Juuti, Hsi Chi-Shiung, Chia Chih-Ta & Jantunen Heli (2015) Dielectric $BaTiO_3$-BBSZ glass ceramic composition with ultra-low sintering temperature. J Euro Ceram Soc 35(1): 139–144.

II Chen Mei-Yu, Juuti Juuti, Hsi Chi-Shiung, Chia Chih-Ta & Jantunen Heli (2015) Dielectric properties of ultra-low sintering temperature Al_2O_3-BBSZ glass composite. J Am Ceram Soc 98(4): 1133–1136.

III Chen Mei-Yu, Juuti Juuti, Hsi Chi-Shiung & Jantunen Heli (2017) Sintering behavior and characteristics study of $BaTiO_3$ with 50 wt% of B_2O_3-Bi_2O_3-SiO_2-ZnO glass. J Euro Ceram Soc 37(4): 1495–1500.

IV Chen Mei-Yu, Vahera Timo, Hsi Chi-Shiung, Sobocinski Maciej, Teirikangas Merja, Peräntie Jani, Juuti Jari, Jantunen Heli (2017) Tape Casting System for ULTCCs to Fabricate Multilayer and Multimaterial 3D Electronic Packages with Embedded Electrodes. J Am Ceram Soc 100(4): 1257-1260.

Original publications are not included in the electronic version of the dissertation.

599. Louis, Jean-Nicolas (2016) Dynamic environmental indicators for smart homes : assessing the role of home energy management systems in achieving decarbonisation goals in the residential sector

600. Mustamo, Pirkko (2017) Greenhouse gas fluxes from drained peat soils : a comparison of different land use types and hydrological site characteristics

601. Upola, Heikki (2017) Disintegration of packaging material : an experimental study of approaches to lower energy consumption

602. Eskelinen, Riku (2017) Runoff generation and load estimation in drained peatland areas

603. Kokkoniemi, Joonas (2017) Nanoscale sensor networks : the THz band as a communication channel

604. Luoto, Petri (2017) Co-primary multi-operator resource sharing for small cell networks

605. Yrjölä, Seppo (2017) Analysis of technology and business antecedents for spectrum sharing in mobile broadband networks

606. Suikkanen, Essi (2017) Detection algorithms and ASIC designs for MIMO–OFDM downlink receivers

607. Niemelä, Ville (2017) Evaluations and analysis of IR-UWB receivers for personal medical communications

608. Keränen, Anni (2017) Water treatment by quaternized lignocellulose

609. Jutila, Mirjami (2017) Adaptive traffic management in heterogeneous communication networks

610. Shahmarichatghieh, Marzieh (2017) Product development sourcing strategies over technology life cycle in high-tech industry

611. Ylitalo, Pekka (2017) Value creation metrics in systematic idea generation

612. Hietajärvi, Anna-Maija (2017) Capabilities for managing project alliances

613. Kangas, Maria (2017) Stability analysis of new paradigms in wireless networks

614. Roivainen, Antti (2017) Three-dimensional geometry-based radio channel model: parametrization and validation at 10 GHz

Book orders:
Granum: Virtual book store
http://granum.uta.fi/granum/

UNIVERSITY OF OULU P.O. Box 8000 FI-90014 UNIVERSITY OF OULU FINLAND

ACTA UNIVERSITATIS OULUENSIS

UNIVERSITY of OULU
OULUN YLIOPISTO

ISBN 978-952-62-1559-4 (Paperback)
ISBN 978-952-62-1560-0 (PDF)
ISSN 0355-3213 (Print)
ISSN 1796-2226 (Online)